Author Accepted Manuscript (AAM)

European Journal of Mechanics - A/Solids

Volume 75, May–June 2019, Pages 355-366

Free vibration and nonlinear dynamic response of imperfect nanocomposite FG-CNTRC double curved shallow shells in thermal environment

Nguyen Dinh Duc[a,b,c]*, Homayoun Hadavinia[d], Tran Quoc Quan[a], Nguyen Dinh Khoa[a]

[a]Advanced Materials and Structures Laboratory, VNU-Hanoi - University of Engineering and Technology (UET), 144 – Xuan Thuy – Cau Giay – Hanoi – Vietnam

[b]Infrastructure Engineering Program -VNU-Hanoi, Vietnam-Japan University (VJU), My Dinh 1 – Tu Liem – Hanoi – Vietnam

[c]National Research Laboratory, Department of Civil and Environmental Engineering, Sejong University, 209 Neungdong-ro, Gwangjin-gu, Seoul 05006, Korea

[d]School of Mechanical & Automotive Engineering, Kingston University, UK

*Corresponding author: Duc N.D.; Email: ducnd@vnu.edu.vn

Abstract: Analytical solutions for the nonlinear vibration of imperfect functionally graded nanocomposite (FG-CNTRC) double curved shallow shells on elastic foundations subjected to mechanical load in thermal environments are introduced in this paper. The double curved shallow shells are reinforced by single-walled carbon nanotubes (SWCNTs) which are assumed to be graded through the thickness direction according to the different types of linear functions. Motion and compatibility equations are derived using Reddy's higher order shear deformation shell theory and taking into account the effects of initial geometrical imperfection and temperature – dependent properties. The deflection – time curve and the natural frequency are determined by using Galerkin method and fourth – order Runge – Kutta method. The effects geometrical parameters, elastic foundations, initial imperfection, temperature increment, mechanical loads and nanotube volume fraction on the nonlinear thermal vibration of the nanocomposite double curved shallow shells are discussed in numerical results. The

accuracy of present approach and theoretical results is verified by some comparisons with the known data in the literature.

Keywords: Nonlinear thermal dynamic and vibration; imperfect nanocomposite FG-CNTRC double curved shallow shell; Galerkin method.

1. Introduction

Advanced materials are generally characterized by unusually high strength fibres with unusually high stiffness, or modulus of elasticity characteristics, compared to other materials, while bound together by weaker matrices. Besides normal advanced materials like ceramic materials, polymers, functionally graded materials (FGM), etc the discovery of carbon nanotubes (CNT) in 1991 opened up a new era in materials science. A CNT is a tube-shaped material, made of carbon, having a diameter measuring on the nanometer scale. Because of the high strength, low weight and high electrical conductivity, CNT open an incredible range of applications in materials science, electronics, chemical processing, energy management, and many other fields. Therefore, the mechanical behaviors of carbon nanotube reinforced structures have attracted much attention of scientists around the world. Patano (Pantano, 2017) investigated the effects of mechanical deformation on electronic transport through multiwall carbon nanotubes. Lv et al. (Lv et al., 2017) implemented molecular dynamics simulations to investigate the effect of single adatom and stone-wales defects on the longitudinal elastic properties of unidirectional carbon nanotube /polypropylene composites. Shen (Shen, 2009) presented an investigation on the nonlinear bending of simply supported, functionally graded nanocomposite plates reinforced by single-walled carbon nanotubes subjected to a transverse uniform or sinusoidal load in thermal environments. Dobrzańska-Danikiewicz et al. (Dobrzańska-Danikiewicz et al., 2017) described the morphology of carbon-metal nanocomposites consisting of nanostructured rhenium permanently attached to carbon nanomaterials, in the form of single-walled, double-walled or multi-walled

carbon nanotubes. Li et al. (Li et al., 2017) studied self nitrogen-doped carbon nanotubes as anode materials for high capacity and cycling stability lithium-ion batteries. Fontananova et al. (Fontananova et al., 2017) focused on effect of functional groups on the properties of multi-walled carbon nanotubes/polyvinylidenefluoride composite membranes. Shen and He (Shen and He, 2017) investigated a large amplitude vibration analysis of nanocomposite doubly curved panels resting on elastic foundations in thermal environments. Duc et al. (Duc et al., 2017) analyzed the thermal and mechanical stability of a functionally graded composite truncated conical shell reinforced by carbon nanotube fibers and surrounded by the elastic foundations. Liu et al. (Liu et al., 2017) prepared antistatic silk fabrics through sericin swelling-fixing treatment with aminated carbon nanotubes. Zghal et al. (Zghal et al., 2017) dealt with linear static analysis of functionally graded carbon nanotube-reinforced composite structures.

Double curved shells can transfer forces very efficiently. Because the thickness to span ratio is very small, very economical and flexible design are easily made and widely used in energy saving constructions such as emergency shelter, cupola of an observatory, roof of a building or an inner courtyard, the shell of a large multi-story building, a sports hall and factory building. Recently, static and dynamic stability, buckling, postbuckling and vibration of double curved shells under different types of loads are important for practical applications and have received considerable interest. Kateryna and Nataliia (Kateryna and Nataliia, 2015) considered stress-deformable state of isotropic double curved shell with internal cracks and a circular hole. Ghosh and Bhattacharya (Ghosh and Bhattacharya, 2015) tried to delve into the modeling of energy transmission through a double-wall curved panel using Green's theorem. Jakomin et al. (Jakomin et al., 2010) discussed stress, deformation and stability conditions for thin double curved shallow bimetallic translation shells. Cortsen et al. (Cortsen et al., 2014) presented research and development results that have lead to a fully automated fabrication cell with two robots, that in one integrated step can produce unique double curved steel reinforcement

structures with sizes up to 2 times 2 meters. Asnafi studied (Asnafi, 2001) theoretically and experimentally the spring back of double curved autobody panels. The static dent resistance performance of the aluminum alloy double-curved panel formed using viscous pressure forming by finite element analysis, which mainly considers the forming process conditions was studied in work of Li and Wang (Li and Wang, 2009). In 2014, Bich et al. (Huy Bich et al., 2014) introduced an analytical approach to investigate the nonlinear dynamic response and vibration of imperfect eccentrically stiffened FGM thick double curved shallow shells on elastic foundation using both the first order shear deformation theory and stress function with full motion equations. Weickgenannt et al. (Weickgenannt et al., 2013) presented a method for optimal sensor placement on shell structures such that the state of oscillation of the system can be reconstructed and model-based methods for active vibration damping can be applied.

Thermal load is defined as the temperature that causes the effect on structures and buildings, such as outdoor air temperature, solar radiation, underground temperature, indoor air temperature and the heat source equipment inside the building. The studies in vibration of structures subjected to thermal load are particularly important in computational mechanics. Dong and Li (Dong and Li, 2017) presented a unified nonlinear analytical solution of bending, buckling and vibration for the temperature-dependent functionally graded rectangular plates subjected to thermal load. Liu et al. (Liu et al., 2013) developed an analytical methodology combining averaging technique of composites and an shape memory alloy constitutive model to determine the transformation properties of the functionally graded – shape memory alloy composite. Bouras and Vrcelj (Bouras and Vrcelj, 2017) performed non-linear elastic pre-buckling and in-plane buckling analysis for a circular shallow concrete arch subjected to a uniformly distributed load and time-varying uniform temperature field. Sha and Wang (Sha and Wang, 2017) implemented thermal-acoustic excitation test and corresponding simulation analysis for clamped metallic thin-walled plate for large deflection strongly nonlinear response problem of thin-walled structure to thermal-acoustic load. To

increase the thermal resistance of various structural components in high temperature environments, Anh et al. (Anh et al., 2015) dealt with nonlinear stability analysis of thin annular spherical shells made of functionally graded materials on elastic foundations under external pressure and temperature. Xu et al. (Xu et al., 2017) studied core-shell cylindrical systems under thermal loads, with the aim to describe possible wrinkling modes, bifurcation diagrams and dimensionless parameters influencing the response of the system. Sheng and Wang (Sheng and Wang, 2017) researched a method to predict the nonlinear dynamic behavior of the fluid-conveying functionally graded cylindrical shell. Han et al. (Han et al., 2017) investigated the free vibration and buckling behaviors of foam-filled composite corrugated sandwich plates under thermal loading. Thai et al. (Thai et al., 2017) used the isogeometric analysis to investigate the post-buckling behavior of functionally graded microplates subjected to mechanical and thermal loads.

Up to date, there are very little researches on mechanical behaviors of nanocomposite FG-CNTRC plates and shells using Reddy's higher order shear deformation theory based on analytical approach because of difficulties in calculations. Therefore, new contribution of the paper is that this is the investigation successfully establish modeling and analytical formulations for the nonlinear dynamic response and vibration of an imperfect shear deformable nanocomposite (FG-CNTRC) double curved shallow shell. The shells are assumed to be resting on elastic foundations and are subjected to the combined action of mechanical, thermal and damping loads. Material properties of nanocomposite double curved shallow shells are assumed to be temperature dependent and graded in the thickness direction according to variety of linear functions. The numerical results are obtained by using Galerkin method and fourth-order Runge-Kutta method. The novelty feature of this study is that achieved results for dynamic response and natural frequency of the shell are presented in the analytical forms. Thus, this study provides fundamental scientific foundations for FG-CNTRC designers, manufacturers and for building projects using FG-CNTRC to select the elements in FG-

CNTRC as well as the parameters of shell structure and foundations to create preeminent loads, thermal resistant capabilities of materials.

2. Modeling

Consider a nanocomposite FG-CNTRC double curved shallow shell of radii of curvature R_x, R_y, length of edges a, b and uniform thickness h resting on elastic foundations in thermal environments. A coordinate system (x, y, z) is established in which (x, y) plane on the middle surface of the shell and z on thickness direction $(-h/2 \le z \le h/2)$ as shown in Fig. 1.

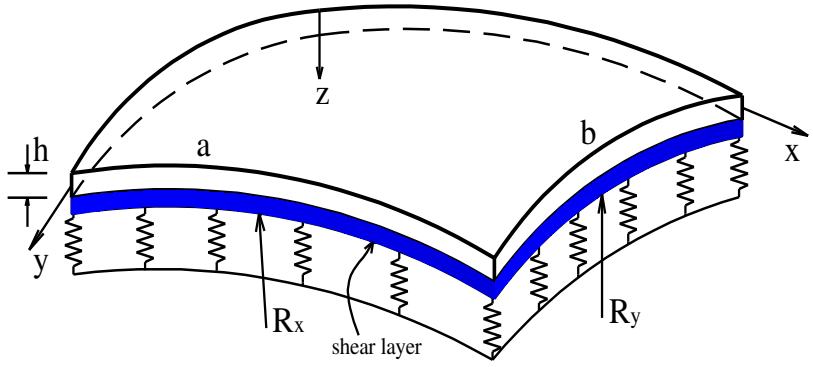

Fig. 1. Geometry and coordinate system of nanocomposite FG-CNTRC double curved shallow shells on elastic foundations.

In this study, the nanocomposite material FG-CNTRC is made of Poly (methyl methacrylate), referred to as PMMA, reinforced by (10,10) SWCNTs. The effective Young's and shear modulus of the FG-CNTRC material are determined are given as (Shen, 2009)

$$\begin{aligned} E_{11} &= \eta_1 V_{CNT} E_{11}^{CNT} + V_m E_m, \\ \frac{\eta_2}{E_{22}} &= \frac{V_{CNT}}{E_{22}^{CNT}} + \frac{V_m}{E_m}, \\ \frac{\eta_3}{G_{12}} &= \frac{V_{CNT}}{G_{12}^{CNT}} + \frac{V_m}{G_m}, \end{aligned} \tag{1}$$

where $E_{11}^{CNT}, E_{22}^{CNT}, G_{12}^{CNT}$ are Young's and shear modulus of the CNT; $E_{m,}\, G_m$ are mechanical properties of the matrix. V_{CNT} and V_m are the volume fractions of the CNT and the matrix, respectively and $\eta_i\ (i=\overline{1,3})$ are the CNT efficiency parameters.

The volume fractions of the CNT and the matrix in nanocomposite are assumed to change according to the variety of linear functions of the shell thickness. Five types of FG-CNTRCs, i.e. UD, FG-O, FG-X, FG-V, and FG-A, are considered and the volume fractions of the three distribution types are expressed specifically as following equations (Shen, 2009)

$$V_{CNT}(z)=\begin{cases} V_{VCT}^{*} & (\ UD\ ) \\ 2V_{VCT}^{*}\left(1-2\dfrac{|z|}{h}\right) & (FG-O) \\ 4V_{VCT}^{*}\dfrac{|z|}{h} & (FG-X)\ , \\ V_{VCT}^{*}\left(1+2\dfrac{z}{h}\right) & (FG-V) \\ V_{VCT}^{*}\left(1-2\dfrac{z}{h}\right) & (FG-\Lambda) \end{cases} \tag{2}$$

$$V_m(z)=1-V_{CNT}(z),$$

where

$$V_{CNT}^{*}=\frac{w_{CNT}}{w_{CNT}+\left(\rho_{CNT}/\rho_m\right)-\left(\rho_{CNT}/\rho_m\right)w_{CNT}}, \tag{3}$$

in which w_{CNT} is the mass fraction of CNTs, and ρ_{CNT} and ρ_m are the densities of CNT and matrix, respectively.

Except Poisson's ratio, the material properties of the matrix are assumed to express as linear functions of temperature (Shen, 2009)

$$\begin{aligned}
&\nu_m = 0.34,\\
&\alpha_m = 45\left(1+0.0005\Delta T\right)\times 10^{-6}/K,\\
&E_m = (3.52-0.0034T)GPa,
\end{aligned} \tag{4}$$

with $T = T_0 + \Delta T$, ΔT is the temperature increment in the environment containing the material and $T_0 = 300K$ (room temperature).

The Young's modulus, shear modulus and thermal expansion coefficient of SWCNTs of (10,10) SWCNTs are highly dependent to temperature as

$$\begin{aligned}
&E_{11}^{CNT}\left[TPa\right] = 6.3998 - 4.33817*10^{-3}T + 7.43*10^{-6}T^2 - 4.45833*10^{-9}T^3,\\
&E_{22}^{CNT}\left[TPa\right] = 8.02155 - 5.420375*10^{-3}T + 9.725*10^{-6}T^2 - 5.5625*10^{-9}T^3,\\
&G_{12}^{CNT}\left[TPa\right] = 1.40755 + 3.476208*10^{-3}T - 6.965*10^{-6}T^2 + 4.479167*10^{-9}T^3,\\
&\alpha_{11}^{CNT}\left[10^{-6}/K\right] = -1.12515 + 0.02291688T - 2.887*10^{-5}T^2 + 1.13625*10^{-8}T^3,\\
&\alpha_{22}^{CNT}\left[10^{-6}/K\right] = 5.43715 - 0.984625*10^{-4}T + 2.9*10^{-7}T^2 - 1.25*10^{-11}T^3,
\end{aligned} \tag{5}$$

and the Poisson's ratio of SWCNTs is chosen to be constant $\nu_{12}^{CNT} = 0.175$.

The CNT efficiency parameters $\eta_i\ (i = \overline{1,3})$ are obtained by the extended rule of mixture to molecular simulation results (Duc et al., 2017; Zghal et al., 2017). For three different volume fraction of CNTs, these parameters are: $\eta_1 = 0.137, \eta_2 = 1.022, \eta_3 = 0.715$ for the case of $V_{CNT}^* = 0.12\ (12\%)$; $\eta_1 = 0.142, \eta_2 = 1.626,\ \eta_3 = 1.138$ for the case of $V_{CNT}^* = 0.17\ (17\%)$ and $\eta_1 = 0.141, \eta_2 = 1.585, \eta_3 = 1.109$ for the case of $V_{CNT}^* = 0.28\ (28\%)$.

The effective Poisson's ratio of nanocomposite FG-CNTRC depends weakly on temperature change and position as (Shen, 2009)

$$\nu_{12} = V_{CNT}^* \nu_{12}^{CNT} + V_m \nu_m, \tag{6}$$

where ν_{12}^{CNT} and ν_m are Poisson's ratio of the CNT and the matrix, respectively.

The thermal expansion coefficients in the longitudinal and transverse directions of the CNTRCs are given by (Shen, 2009)

$$\alpha_{11} = \frac{V_{CNT} E_{11}^{CNT} \alpha_{11}^{CNT} + V_m E_m \alpha_m}{V_{CNT} E_{11}^{CNT} + V_m E_m},$$
$$\alpha_{22} = (1+\nu_{12}^{CNT}) V_{CNT} \alpha_{22}^{CNT} + (1+\nu_m) V_m \alpha_m - \nu_{12} \alpha_{11}, \tag{7}$$

with $\alpha_{11}^{CNT}, \alpha_{22}^{CNT}$ and α_m are the thermal expansion coefficients of the CNT and the matrix, respectively.

3. Basic equations

In this study, the Reddy's higher order shear deformation shell theory (Brush and Almroth, 1975; Reddy, 2004) is used to establish governing equations and to determine the nonlinear vibration and dynamic response of imperfect FG-CNTRC thick double curved shallow shells in thermal environments.

The relationship of strains and displacements taking into account the von Karman nonlinear terms are (Brush and Almroth, 1975; Reddy, 2004)

$$\begin{pmatrix} \varepsilon_x \\ \varepsilon_y \\ \gamma_{xy} \end{pmatrix} = \begin{pmatrix} \varepsilon_x^0 \\ \varepsilon_y^0 \\ \gamma_{xy}^0 \end{pmatrix} + z \begin{pmatrix} k_x^1 \\ k_y^1 \\ k_{xy}^1 \end{pmatrix} + z^3 \begin{pmatrix} k_x^3 \\ k_y^3 \\ k_{xy}^3 \end{pmatrix}, \begin{pmatrix} \gamma_{xz} \\ \gamma_{yz} \end{pmatrix} = \begin{pmatrix} \gamma_{xz}^0 \\ \gamma_{yz}^0 \end{pmatrix} + z^2 \begin{pmatrix} k_{xz}^2 \\ k_{yz}^2 \end{pmatrix}, \tag{8}$$

in which

$$\begin{pmatrix} k_x^1 \\ k_y^1 \\ k_{xy}^1 \end{pmatrix} = \begin{pmatrix} \dfrac{\partial \phi_x}{\partial x} \\ \dfrac{\partial \phi_y}{\partial y} \\ \dfrac{\partial \phi_x}{\partial y} + \dfrac{\partial \phi_y}{\partial x} \end{pmatrix}, \begin{pmatrix} k_x^3 \\ k_y^3 \\ k_{xy}^3 \end{pmatrix} = -c_1 \begin{pmatrix} \dfrac{\partial \phi_x}{\partial x} + \dfrac{\partial^2 w}{\partial x^2} \\ \dfrac{\partial \phi_y}{\partial y} + \dfrac{\partial^2 \mathrm{w}}{\partial y^2} \\ \dfrac{\partial \phi_x}{\partial y} + \dfrac{\partial \phi_y}{\partial x} + 2\dfrac{\partial^2 \mathrm{w}}{\partial x \partial y} \end{pmatrix}, \tag{9}$$

$$\begin{pmatrix}\varepsilon_x^0\\ \varepsilon_y^0\\ \gamma_{xy}^0\end{pmatrix}=\begin{pmatrix}\dfrac{\partial u}{\partial x}-\dfrac{w}{R_x}+\dfrac{1}{2}\left(\dfrac{\partial w}{\partial x}\right)^2\\ \dfrac{\partial v}{\partial y}-\dfrac{w}{R_y}+\dfrac{1}{2}\left(\dfrac{\partial w}{\partial y}\right)^2\\ \dfrac{\partial u}{\partial y}+\dfrac{\partial v}{\partial x}+\dfrac{\partial w}{\partial x}\dfrac{\partial w}{\partial y}\end{pmatrix},\begin{pmatrix}\gamma_{xz}^0\\ \gamma_{yz}^0\end{pmatrix}=\begin{pmatrix}\phi_x+\dfrac{\partial \mathrm{w}}{\partial x}\\ \phi_y+\dfrac{\partial \mathrm{w}}{\partial y}\end{pmatrix};\begin{pmatrix}k_{xz}^2\\ k_{yz}^2\end{pmatrix}=-3c_1\begin{pmatrix}\phi_x+\dfrac{\partial \mathrm{w}}{\partial x}\\ \phi_y+\dfrac{\partial \mathrm{w}}{\partial y}\end{pmatrix},$$

and $c_1=\dfrac{4}{3h^2}$; u,v,w are displacement components corresponding to the coordinates (x,y,z), ϕ_x,ϕ_y are the slopes of the transverse normal about the x and y axes at $z=0$.

Hooke law for a nanocomposite FG-CNTRC double curved shallow shell including temperature effect is defined as (Duc et al., 2017; Zghal et al., 2017; Quan and Duc, 2017)

$$\begin{bmatrix}\sigma_{xx}\\ \sigma_{yy}\\ \sigma_{xy}\\ \sigma_{xz}\\ \sigma_{yz}\end{bmatrix}=\begin{bmatrix}Q_{11} & Q_{12} & 0 & 0 & 0\\ Q_{12} & Q_{22} & 0 & 0 & 0\\ 0 & 0 & Q_{66} & 0 & 0\\ 0 & 0 & 0 & Q_{44} & 0\\ 0 & 0 & 0 & 0 & Q_{55}\end{bmatrix}\begin{bmatrix}\varepsilon_{xx}-\alpha_{11}\Delta T\\ \varepsilon_{yy}-\alpha_{22}\Delta T\\ \varepsilon_{xy}\\ \varepsilon_{xz}\\ \varepsilon_{yz}\end{bmatrix},\tag{10}$$

where

$$Q_{11}=\frac{E_{11}}{1-\nu_{12}\nu_{21}},\ Q_{22}=\frac{E_{22}}{1-\nu_{12}\nu_{21}},\ Q_{12}=\frac{\nu_{21}E_{11}}{1-\nu_{12}\nu_{21}},\ Q_{44}=G_{23},\ Q_{55}=G_{13},\ Q_{66}=G_{12}.\tag{11}$$

and we use an assumption that $G_{13}=G_{12}$ and $G_{23}=1.2G_{12}$.

The force and moment resultants of FG-CNTRC double curved shallow shells are given by

$$\begin{aligned}
&\left(N_i, M_i, P_i\right) = \int_{-h/2}^{h/2} \sigma_i (1, z, z^3) dz,\ i = x, y, xy, \\
&\left(Q_i, K_i\right) = \int_{-h/2}^{h/2} \sigma_{iz} (1, z^2) dz,\ i = x, y.
\end{aligned} \tag{12}$$

Introduction of Eqs. (8) and (9) into Eq. (10) and the results into Eq. (12) give the constitutive relations as

$$\begin{aligned}
N_x &= A_{11}\varepsilon_x^0 + A_{12}\varepsilon_y^0 + B_{11}k_x^1 + B_{12}k_y^1 + D_{11}k_x^3 + D_{12}k_y^3 - \left(\Phi_a^1 + \Phi_a^2\right)\Delta T, \\
N_y &= A_{12}\varepsilon_x^0 + A_{22}\varepsilon_y^0 + B_{12}k_x^1 + B_{22}k_y^1 + D_{12}k_x^3 + D_{22}k_y^3 - \left(\Phi_a^3 + \Phi_a^4\right)\Delta T, \\
N_{xy} &= A_{66}\gamma_{xy}^0 + B_{66}k_{xy}^1 + D_{66}k_{xy}^3, \\
M_x &= B_{11}\varepsilon_x^0 + B_{12}\varepsilon_y^0 + C_{11}k_x^1 + C_{12}k_y^1 + E_{11}k_x^3 + E_{12}k_y^3 - \left(\Phi_b^1 + \Phi_b^2\right)\Delta T, \\
M_y &= B_{12}\varepsilon_x^0 + B_{22}\varepsilon_y^0 + C_{12}k_x^1 + C_{22}k_y^1 + E_{12}k_x^3 + E_{22}k_y^3 - \left(\Phi_b^3 + \Phi_b^4\right)\Delta T, \\
M_{xy} &= B_{66}\gamma_{xy}^0 + C_{66}k_{xy}^1 + E_{66}k_{xy}^3, \\
P_x &= D_{11}\varepsilon_x^0 + D_{12}\varepsilon_y^0 + E_{11}k_x^1 + E_{12}k_y^1 + G_{11}k_x^3 + G_{12}k_y^3 - \left(\Phi_c^1 + \Phi_c^2\right)\Delta T, \\
P_y &= D_{12}\varepsilon_x^0 + D_{22}\varepsilon_y^0 + E_{12}k_x^1 + E_{22}k_y^1 + G_{12}k_x^3 + G_{22}k_y^3 - \left(\Phi_c^3 + \Phi_c^4\right)\Delta T, \\
P_{xy} &= D_{66}\gamma_{xy}^0 + E_{66}k_{xy}^1 + G_{66}k_{xy}^3, \\
Q_x &= A_{44}\gamma_{xz}^0 + C_{44}k_{xz}^2, \\
Q_y &= A_{55}\gamma_{yz}^0 + C_{55}k_{yz}^2, \\
K_x &= C_{44}\gamma_{xz}^0 + E_{44}k_{xz}^2, \\
K_y &= C_{55}\gamma_{yz}^0 + E_{55}k_{yz}^2,
\end{aligned} \tag{13}$$

in which

$$\left(A_{ij}, B_{ij}, C_{ij}, D_{ij}, E_{ij}, G_{ij}\right) = \int_{-h/2}^{h/2} Q_{ij}(1, z, z^2, z^3, z^4, z^6)\,dz,\ ij = 11,12,22,66,$$

$$(A_{kl}, C_{kl}, E_{kl}) = \int_{-h/2}^{h/2} Q_{ij}(1, z^2, z^4)\,dz,\ kl = 44,55,$$

$$(\Phi_a^1, \Phi_a^2, \Phi_a^3, \Phi_a^4) = \int_{-h/2}^{h/2} (Q_{11}\alpha_{11}, Q_{12}\alpha_{22}, Q_{12}\alpha_{11}, Q_{22}\alpha_{22})dz,$$

$$(\Phi_b^1, \Phi_b^2, \Phi_b^3, \Phi_b^4) = \int_{-h/2}^{h/2} (Q_{11}\alpha_{11}, Q_{12}\alpha_{22}, Q_{12}\alpha_{11}, Q_{22}\alpha_{22})zdz, \tag{14}$$

$$(\Phi_c^1, \Phi_c^2, \Phi_c^3, \Phi_c^4) = \int_{-h/2}^{h/2} (Q_{11}\alpha_{11}, Q_{12}\alpha_{22}, Q_{12}\alpha_{11}, Q_{22}\alpha_{22})z^3dz.$$

From the constitutive relations in Eq. (13), one can write

$$\begin{aligned}
&\varepsilon_x^0 = A_{22}^* N_x - A_{21}^* N_y - B_{21}^* k_x^1 - B_{22}^* k_y^1 - D_{21}^* k_x^3 \\
&- D_{22}^* k_y^3 + \left[A_{22}^*\left(\Phi_a^1 + \Phi_a^2\right) - A_{21}^*\left(\Phi_a^3 + \Phi_a^4\right)\right]\Delta T, \\
&\varepsilon_y^0 = A_{11}^* N_x - A_{12}^* N_y + B_{11}^* k_x^1 + B_{12}^* k_y^1 + D_{11}^* k_x^3 \\
&+ D_{12}^* k_y^3 - \left[A_{12}^*\left(\Phi_a^1 + \Phi_a^2\right) - A_{11}^*\left(\Phi_a^3 + \Phi_a^4\right)\right]\Delta T, \\
&\gamma_{xy}^0 = A_{66}^* N_{xy} - B_{66}^* k_{xy}^1 - D_{66}^* k_{xy}^3,
\end{aligned} \tag{15}$$

where

$$\begin{aligned}
&\Delta = A_{11}A_{22} - A_{12}^2,\ A_{11}^* = \frac{A_{11}}{\Delta},\ A_{12}^* = A_{21}^* = \frac{A_{12}}{\Delta},\ A_{22}^* = \frac{A_{22}}{\Delta},\ B_{21}^* = \frac{A_{22}B_{11} - A_{12}B_{12}}{\Delta}, \\
&B_{22}^* = \frac{A_{22}B_{12} - A_{12}B_{22}}{\Delta},\ B_{11}^* = \frac{A_{12}B_{11} - A_{11}B_{12}}{\Delta},\ B_{12}^* = \frac{A_{12}B_{12} - A_{11}B_{22}}{\Delta}, \\
&D_{21}^* = \frac{A_{22}D_{11} - A_{12}D_{12}}{\Delta},\ D_{22}^* = \frac{A_{22}D_{12} - A_{12}D_{22}}{\Delta},\ D_{11}^* = \frac{A_{12}D_{11} - A_{11}D_{12}}{\Delta}, \\
&D_{12}^* = \frac{A_{12}D_{12} - A_{11}D_{22}}{\Delta},\ A_{66}^* = \frac{1}{A_{66}},\ B_{66}^* = \frac{B_{66}}{A_{66}},\ D_{66}^* = \frac{D_{66}}{A_{66}}.
\end{aligned} \tag{16}$$

Based on the higher order shear deformation theory, the nonlinear motion equations of an imperfect FG-CNTRC double curved shallow shells are defined by (Reddy, 2004)

$$\frac{\partial N_x}{\partial x}+\frac{\partial N_{xy}}{\partial y}=\overline{I}_1\frac{\partial^2 u}{\partial t^2}+\overline{I}_2\frac{\partial^2 \phi_x}{\partial t^2}-\overline{I}_3\frac{\partial^3 w}{\partial t^2\partial x}, \tag{17a}$$

$$\frac{\partial N_{xy}}{\partial x}+\frac{\partial N_y}{\partial y}=\overline{I}_1^*\frac{\partial^2 v}{\partial t^2}+\overline{I}_2^*\frac{\partial^2 \phi_y}{\partial t^2}-\overline{I}_3^*\frac{\partial^3 w}{\partial t^2\partial y}, \tag{17b}$$

$$\begin{aligned}&\frac{\partial Q_x}{\partial x}+\frac{\partial Q_y}{\partial y}-3c_1\left(\frac{\partial R_x}{\partial x}+\frac{\partial R_y}{\partial y}\right)+c_1\left(\frac{\partial^2 P_x}{\partial x^2}+2\frac{\partial^2 P_y}{\partial x\partial y}+\frac{\partial^2 P_y}{\partial y^2}\right)+\frac{N_x}{R_x}+\frac{N_y}{R_y}+q+N_x\frac{\partial^2 w}{\partial x^2}\\&+2N_{xy}\frac{\partial^2 w}{\partial x\partial y}+N_y\frac{\partial^2 w}{\partial y^2}-k_1 w+k_2\nabla^2 w=I_1\frac{\partial^2 w}{\partial t^2}+2\varepsilon I_1\frac{\partial w}{\partial t}+\overline{I}_3\frac{\partial^3 u}{\partial t^2\partial x}+\overline{I}_5\frac{\partial^3 \phi_x}{\partial t^2\partial x}\\&+\overline{I}_3^*\frac{\partial^3 v}{\partial t^2\partial y}+\overline{I}_5^*\frac{\partial^3 \phi_y}{\partial t^2\partial y}-c_1^2 I_7\left(\frac{\partial^4 w}{\partial t^2\partial x^2}+\frac{\partial^4 w}{\partial t^2\partial y^2}\right),\end{aligned} \tag{17c}$$

$$\frac{\partial M_x}{\partial x}+\frac{\partial M_{xy}}{\partial y}-Q_x+3c_1R_x-c_1\left(\frac{\partial P_x}{\partial x}+\frac{\partial P_{xy}}{\partial y}\right)=\overline{I}_2\frac{\partial^2 u}{\partial t^2}+\overline{I}_4\frac{\partial^2 \phi_x}{\partial t^2}-\overline{I}_5\frac{\partial^3 w}{\partial t^2\partial x}, \tag{17d}$$

$$\frac{\partial M_{xy}}{\partial x}+\frac{\partial M_y}{\partial y}-Q_y+3c_1R_y-c_1\left(\frac{\partial P_{xy}}{\partial x}+\frac{\partial P_y}{\partial y}\right)=\overline{I}_2^*\frac{\partial^2 v}{\partial t^2}+\overline{I}_4^*\frac{\partial^2 \phi_y}{\partial t^2}-\overline{I}_5^*\frac{\partial^3 w}{\partial t^2\partial y}, \tag{17e}$$

in which k_1 is the Winkler foundation modulus, k_2 is the shear layer foundation stiffness of the Pasternak model, q is an external pressure uniformly distributed on the surface of the panel, ε is the viscous damping coefficient and

$$\begin{aligned}&\overline{I}_1=I_1+\frac{2I_2}{R_x},\ \overline{I}_1^*=I_1+\frac{2I_2}{R_y},\ \overline{I}_2=I_2+\frac{I_3}{R_x}-c_1I_4-\frac{c_1I_5}{R_x},\ \overline{I}_2^*=I_2+\frac{I_3}{R_y}-c_1I_4-\frac{c_1I_5}{R_y},\\&\overline{I}_3=c_1I_4+\frac{c_1I_5}{R_x},\ \overline{I}_3^*=c_1I_4+\frac{c_1I_5}{R_y},\ \overline{I}_4=\overline{I}_4^*=I_3-2c_1I_5+c_1^2I_7,\ \overline{I}_5=\overline{I}_5^*=c_1I_5-c_1^2I_7,\\&\left(I_1,I_2,I_3,I_4,I_5,I_7\right)=\int_{-h/2}^{h/2}\rho(z)\left(1,z,z^2,z^3,z^4,z^6\right)dz,\\&\rho(z)=V_{CNT}\rho_{CNT}+V_m\rho_m.\end{aligned} \tag{18}$$

The Airy stress function $f\left(x,y,t\right)$ is defined as

$$N_x=\frac{\partial^2 f}{\partial y^2},\ N_y=\frac{\partial^2 f}{\partial x^2},\ N_{xy}=-\frac{\partial^2 f}{\partial x\partial y}. \tag{19}$$

Substituting Eq. (19) into Eqs. (17a) and (17b) gives

$$\frac{\partial^2 u}{\partial t^2} = -\frac{\overline{I_2}}{\overline{I_1}}\frac{\partial^2 \phi_x}{\partial t^2} + \frac{\overline{I_3}}{\overline{I_1}}\frac{\partial^3 w}{\partial t^2 \partial x}, \tag{20a}$$

$$\frac{\partial^2 v}{\partial t^2} = -\frac{\overline{I_2^*}}{\overline{I_1^*}}\frac{\partial^2 \phi_y}{\partial t^2} + \frac{\overline{I_3^*}}{\overline{I_1^*}}\frac{\partial^3 w}{\partial t^2 \partial y}. \tag{20b}$$

Inserting Eqs. (20a) and (20b) into Eqs. (17c), (17d) and (17e) yields

$$\begin{aligned}
&Q_{x,x} + Q_{y,y} - 3c_1\left(K_{x,x} + K_{y,y}\right) + c_1\left(P_{x,xx} + 2P_{xy,xy} + P_{y,yy}\right) + \frac{f_{,yy}}{R_x} + \frac{f_{,xx}}{R_y} + q + f_{,yy}w_{,xx} \\
&-2f_{,xy}w_{,xy} + f_{,xx}w_{,yy} - k_1 w + k_2\nabla^2 w = I_1\frac{\partial^2 w}{\partial t^2} + 2\varepsilon I_1\frac{\partial w}{\partial t} + \overline{\overline{I_5}}\frac{\partial^3 \phi_x}{\partial t^2 \partial x} + \overline{\overline{I_5^*}}\frac{\partial^3 \phi_y}{\partial t^2 \partial x} \\
&+\overline{\overline{I_7}}\frac{\partial^4 w}{\partial t^2 \partial x^2} + \overline{\overline{I_7^*}}\frac{\partial^4 w}{\partial t^2 \partial y^2}, \\
&M_{x,x} + M_{xy,y} - Q_x + 3c_1 K_x - c_1\left(P_{x,x} + P_{xy,y}\right) = \overline{\overline{I_3}}\frac{\partial^2 \phi_x}{\partial t^2} - \overline{\overline{I_5}}\frac{\partial^3 w}{\partial t^2 \partial x}, \\
&M_{xy,x} + M_{y,y} - Q_y + 3c_1 K_y - c_1\left(P_{xy,x} + P_{y,y}\right) = \overline{\overline{I_3^*}}\frac{\partial^2 \phi_y}{\partial t^2} - \overline{\overline{I_5^*}}\frac{\partial^3 w}{\partial t^2 \partial y},
\end{aligned} \tag{21}$$

in which

$$\begin{aligned}
&\overline{\overline{I_3}} = \overline{I_4} - \left(\overline{I_2}\right)^2 / \overline{I_1},\ \overline{\overline{I_3^*}} = \overline{I_4^*} - \left(\overline{I_2^*}\right)^2 / \overline{I_1^*},\ \overline{\overline{I_5}} = \overline{I_5} - \overline{I_2}\,\overline{I_3} / \overline{I_1},\ \overline{\overline{I_5^*}} = \overline{I_5^*} - \overline{I_2^*}\,\overline{I_3^*} / \overline{I_1^*} \\
&\overline{\overline{I_7}} = \left(\overline{I_3}\right)^2 / \overline{I_1} - c_1^2 I_7,\ \overline{\overline{I_7^*}} = \left(\overline{I_3^*}\right)^2 / \overline{I_1^*} - c_1^2 I_7.
\end{aligned} \tag{22}$$

Replacing Eqs. (15) and (19) into Eq. (13) and then into Eqs. (21), we have

$$\begin{aligned}
&H_{11}(w) + H_{12}(\phi_x) + H_{13}(\phi_y) + H_{14}(f) + P(w,f) + q, \\
&= I_1\frac{\partial^2 w}{\partial t^2} + 2\varepsilon I_1\frac{\partial w}{\partial t} + \overline{\overline{I_5}}\frac{\partial^3 \phi_x}{\partial t^2 \partial x} + \overline{\overline{I_5^*}}\frac{\partial^3 \phi_y}{\partial t^2 \partial x} + \overline{\overline{I_7}}\frac{\partial^4 w}{\partial t^2 \partial x^2} + \overline{\overline{I_7^*}}\frac{\partial^4 w}{\partial t^2 \partial y^2} \\
&H_{21}(w) + H_{22}(\phi_x) + H_{23}(\phi_y) + H_{24}(f) = \overline{\overline{I_3}}\frac{\partial^2 \phi_x}{\partial t^2} - \overline{\overline{I_5}}\frac{\partial^3 w}{\partial t^2 \partial x}, \\
&H_{31}(w) + H_{32}(\phi_x) + H_{32}(\phi_y) + H_{34}(f) = \overline{\overline{I_3^*}}\frac{\partial^2 \phi_y}{\partial t^2} - \overline{\overline{I_5^*}}\frac{\partial^3 w}{\partial t^2 \partial y},
\end{aligned} \tag{23}$$

where

$$
\begin{aligned}
&H_{11}(w) = X_{11}w_{,xx} + X_{12}w_{,yy} + X_{13}w_{,xxxx} + X_{14}w_{,xxyy} + X_{15}w_{,yyyy} - k_1 w + k_2\nabla^2 w,\\
&H_{12}(\phi_x) = X_{11}\phi_{x,x} + X_{16}\phi_{x,xxx} + X_{17}\phi_{x,xyy},\\
&H_{13}(\phi_y) = X_{12}\phi_{y,y} + X_{18}\phi_{y,yyy} + X_{19}\phi_{y,xxy},\\
&H_{14}(f) = X_{110}f_{,xxxx} + X_{111}f_{,xxyy} + X_{112}f_{,yyyy} + \frac{f_{,yy}}{R_x} + \frac{f_{,xx}}{R_y},\\
&P(w,f) = f_{,yy}w_{,xx} - 2f_{,xy}w_{,xy} + f_{,xx}w_{,yy},\\
&H_{21}(w) = X_{21}w_{,x} + X_{22}w_{,xxx} + X_{23}w_{,xyy},\\
&H_{22}(\phi_x) = X_{21}\phi_x + X_{24}\phi_{x,xx} + X_{25}\phi_{x,yy},\\
&H_{23}(\phi_y) = X_{26}\phi_{y,xy},\\
&H_{24}(f) = X_{27}f_{,xxx} + X_{28}f_{,xyy},\\
&H_{31}(w) = X_{31}w_{,y} + X_{32}w_{,xxy} + X_{33}w_{,yyy},\\
&H_{32}(\phi_x) = X_{34}\phi_{x,xy},\\
&H_{33}(\phi_y) = X_{31}\phi_y + X_{35}\phi_{y,xx} + X_{36}\phi_{y,yy},\\
&H_{34}(f) = X_{37}f_{,xxy} + X_{38}f_{,yyy},
\end{aligned}
\tag{24}
$$

with and the detail of coefficients $X_{1i}(i=\overline{1,12})$, $X_{2j}(j=\overline{1,8})$, $X_{3k}(k=\overline{1,8})$ are given in Appendix A.

The initial imperfection of the nanocomposite (FG-CNTRC) double curved shallow shells can be seen as a small deviation of middle surface of the shell from the perfect shape, also seen as an initial deflection which is very small compared with the shell dimensions, but may be compared with the shell wall thickness. Let $w^*(x,y)$ denote a known small imperfection, Eq. (23) can be rewritten as the following form

$$
\begin{aligned}
&H_{11}(w) + H_{12}(\phi_x) + H_{13}(\phi_y) + H_{14}(f) + P(w,f) + H_{11}^*(w^*) + P^*(w^*,f) + q\\
&= I_1\frac{\partial^2 w}{\partial t^2} + 2\varepsilon I_1\frac{\partial w}{\partial t} + \overline{=}{I}_5\frac{\partial^3\phi_x}{\partial t^2\partial x} + \overline{=}{I}_5^*\frac{\partial^3\phi_y}{\partial t^2\partial x} + \overline{=}{I}_7\frac{\partial^4 w}{\partial t^2\partial x^2} + \overline{=}{I}_7^*\frac{\partial^4 w}{\partial t^2\partial y^2},\\
&H_{21}(w) + H_{22}(\phi_x) + H_{23}(\phi_y) + H_{24}(f) + H_{21}^*(w^*) = \overline{=}{I}_3\frac{\partial^2\phi_x}{\partial t^2} - \overline{=}{I}_5\frac{\partial^3 w}{\partial t^2\partial x},
\end{aligned}
\tag{25}
$$

$$H_{31}(w)+H_{32}(\phi_x)+H_{32}(\phi_y)+H_{34}(f)+H_{31}^{*}(w^{*})=\overline{\overline{I}}_3^{*}\frac{\partial^2\phi_y}{\partial t^2}-\overline{\overline{I}}_5^{*}\frac{\partial^3 w}{\partial t^2\partial y},$$

in which

$$\begin{aligned}
&H_{11}^{*}(w^{*})=X_{11}w_{,xx}^{*}+X_{12}w_{,yy}^{*}+X_{13}w_{,xxxx}^{*}V_{31}+X_{14}w_{,xxyy}^{*}+X_{15}w_{,yyyy}^{*},\\
&P^{*}(w^{*},f)=f_{,yy}w_{,xx}^{*}-2f_{,xy}w_{,xy}^{*}+f_{,xx}w_{,yy}^{*},\\
&H_{21}^{*}(w^{*})=X_{21}w_{,x}^{*}+X_{22}w_{,xxx}^{*}+X_{23}w_{,xyy}^{*},\\
&H_{31}^{*}(w^{*})=X_{31}w_{,y}^{*}+X_{32}w_{,xxy}^{*}+X_{33}w_{,yyy}^{*}.
\end{aligned}\tag{26}$$

The geometrical compatibility equation for an imperfect nanocomposite (FG-CNTRC) double curved shallow shell may be derived as (Quan and Duc, 2017; Duc and Quan, 2015; Duc, 213)

$$\varepsilon_{x,yy}^{0}+\varepsilon_{y,xx}^{0}-\gamma_{xy,xy}^{0}=w_{,xy}^{2}-w_{,xx}w_{,yy}+2w_{,xy}w_{,xy}^{*}-w_{,xx}w_{,yy}^{*}-w_{,yy}w_{,xx}^{*}-\frac{w_{,yy}}{R_x}-\frac{w_{,xx}}{R_y}.\tag{27}$$

Setiing Eqs. (15) and (19) into the Eq. (27) gives

$$\begin{aligned}
&A_{11}^{*}f_{,xxxx}+A_{22}^{*}f_{,yyyy}+\left(A_{66}^{*}-A_{21}^{*}+A_{12}^{*}\right)f_{,xxyy}+\left(B_{11}^{*}-c_1D_{11}^{*}\right)\phi_{x,xxx}+\left(c_1D_{22}^{*}-B_{22}^{*}\right)\phi_{y,yyy}\\
&+\left(B_{66}^{*}+c_1D_{21}^{*}-B_{21}^{*}-c_1D_{66}^{*}\right)\phi_{x,xyy}+\left(B_{66}^{*}+B_{12}^{*}-c_1D_{12}^{*}-c_1D_{66}^{*}\right)\phi_{y,xxy}\\
&-c_1D_{11}^{*}w_{,xxxx}+c_1D_{22}^{*}w_{,yyyy}+\left(c_1D_{21}^{*}-c_1D_{12}^{*}-2c_1D_{66}^{*}\right)w_{,xxyy}\\
&=w_{,xy}^{2}-w_{,xx}w_{,yy}+2w_{,xy}w_{,xy}^{*}-w_{,xx}w_{,yy}^{*}-w_{,yy}w_{,xx}^{*}-\frac{w_{,yy}}{R_x}-\frac{w_{,xx}}{R_y}.
\end{aligned}\tag{28}$$

Eqs. (25) and (28) are nonlinear equations in terms of variables w,ϕ_x,ϕ_y and f, and are used to investigate the nonlinear vibration and dynamic response of the imperfect FG-CNTRC thick double curved shallow shells using the higher order shear deformation shell theory.

4. Nonlinear vibration analysis

4.1. Boundary conditions and solutions

The imperfect FG-CNTRC double curved shallow shell is subjected to uniformly distributed pressure of intensity q (Pascals) and simultaneously exposed to temperature environments. Four edges of the shell are assumed to be simply supported and immovable. The boundary conditions are defined as

$$\begin{aligned} &w = u = \phi_y = M_x = P_x = 0,\ N_x = N_{x0}\ at\ \ x = 0, a, \\ &w = v = \phi_x = M_y = P_y = 0,\ N_y = N_{y0}\ at\ \ y = 0, b, \end{aligned} \tag{29}$$

with N_{x0}, N_{y0} are fictitious compressive loads at immovable edges.

The following approximate solution is chosen to satisfy the boundary conditions

$$\begin{aligned} &w(x, y, \mathrm{t}) = W(t)\sin\alpha x \sin\beta y, \\ &\phi_x(x, y, \mathrm{t}) = \Phi_x(t)\cos\alpha x \sin\beta y, \\ &\phi_y(x, y, \mathrm{t}) = \Phi_y(t)\sin\alpha x \cos\beta y, \end{aligned} \tag{30}$$

where $\alpha = m\pi / a$, $\beta = n\pi / b$; m, n are odd natural numbers representing the number of half waves in the x and y directions, respectively; and $W(t), \Phi_x, \Phi_y$ are the time dependent amplitudes.

The initial imperfection of the FG-CNTRC double curved shallow shell is assumed to have the form like the shell deflection, i.e.

$$w^*(x, y) = W_0 \sin\alpha x \sin\beta y. \tag{31}$$

The Airy stress function is obtained by putting Eqs. (30) and (31) into Eq. (28) as

$$f\left(x,y,t\right)=A_1\left(t\right)\cos 2\alpha x+A_2\left(t\right)\cos 2\beta y$$
$$+A_3\left(t\right)\sin\alpha x\sin\beta y+\frac{1}{2}N_{x0}y^2+\frac{1}{2}N_{y0}x^2, \tag{32}$$

in which

$$A_1=\frac{\beta^2}{32\alpha^2A_{11}^*}W\left(W+2W_0\right),$$
$$A_2=\frac{\alpha^2}{32\beta^2A_{22}^*}W\left(W+2W_0\right), \tag{33}$$
$$A_3=\frac{H_2}{H_1}\Phi_x+\frac{H_3}{H_1}\Phi_y+\frac{H_4}{H_1}W,$$

and

$$H_1=A_{11}^*\alpha^4+A_{22}^*\beta^4+\left(A_{66}^*-A_{21}^*-A_{12}^*\right)\alpha^2\beta^2,$$
$$H_2=-\left(B_{11}^*-c_1D_{11}^*\right)\alpha^3-\left(B_{66}^*+c_1D_{21}^*-B_{21}^*-c_1D_{66}^*\right)\alpha\beta^2,$$
$$H_3=-\left(c_1D_{22}^*-B_{22}^*\right)\beta^3-\left(B_{66}^*+B_{12}^*-c_1D_{12}^*-c_1D_{66}^*\right)\alpha^2\beta, \tag{34}$$
$$H_4=\left(\frac{\beta^2}{R_x}+\frac{\alpha^2}{R_y}\right)-\left[c_1D_{22}^*\beta^4-c_1D_{11}^*\alpha^4+\left(c_1D_{21}^*-c_1D_{12}^*-2c_1D_{66}^*\right)\alpha^2\beta^2\right].$$

4.2. Nonlinear dynamic response

Subsequently, replacing Eqs. (30) - (32) into Eqs. (25) and then applying Galerkin method to the resulting equations yields

$$J_{11}W+J_{12}\Phi_x\left(t\right)+J_{13}\Phi_y\left(t\right)+J_{14}\Phi_x\left(W+W_0\right)+J_{15}\Phi_y\left(W+W_0\right)$$
$$+\left(n_1-\alpha^2N_{x0}-\beta^2N_{y0}\right)\left(W+W_0\right)+n_2W\left(W+W_0\right)$$
$$+n_3W\left(W+2W_0\right)+n_4W\left(W+2W_0\right)\left(W+W_0\right) \tag{35a}$$
$$+n_5\left(\frac{1}{R_x}N_{x0}+\frac{1}{R_y}N_{y0}\right)+n_5q=I_1\frac{\partial^2W}{\partial t^2}+2\varepsilon I_1\frac{\partial W}{\partial t}-\alpha\overline{\overline{I}}_5\frac{\partial^2\Phi_x}{\partial t^2}-\beta\overline{\overline{I}}_5^*\frac{\partial^2\Phi_y}{\partial t^2},$$

$$J_{21}W+J_{22}\Phi_x\left(t\right)+J_{23}\Phi_y\left(t\right)+n_6\left(W+W_0\right)+n_7W\left(W+2W_0\right)=\overline{\overline{I}}_3\frac{\partial^2\Phi_x}{\partial t^2}-\alpha\overline{\overline{I}}_5\frac{\partial^2W}{\partial t^2}, \tag{35b}$$

$$J_{31}W + J_{32}\Phi_x(t) + J_{33}\Phi_y(t) + n_8(W + W_0) + n_9 W(W + 2W_0) = \overline{\overline{I_3^*}}\frac{\partial^2 \Phi_y}{\partial t^2} - \beta \overline{\overline{I_5^*}}\frac{\partial^2 W}{\partial t^2}, \tag{35c}$$

where the details of coefficients $J_{1i}(i = \overline{1,5})$, $J_{2j}(j = \overline{1,3})$, $J_{3k}(k = \overline{1,3}), n_q(q = \overline{1,9})$ may be found in Appendix B.

These are basic equations to determine the nonlinear dynamic response and natural frequency of imperfect thick nanocomposite FG-CNTRC double curved shallow shell in thermal environments.

The in-plane condition on immovability at all edges of nanocomposite double curved shallow shell, ie. $u = 0$ at $x = 0, a$ and $v = 0$ at $y = 0, b$, is fulfilled in an average sense as

$$\int_0^b \int_0^a \frac{\partial u}{\partial x} dxdy = 0, \int_0^a \int_0^b \frac{\partial v}{\partial y} dydx = 0. \tag{36}$$

We can give the following expression from Eqs. (9) and (15) in which initial imperfection of the shell and Eq. (19) are taken into account

$$\begin{aligned}
&\frac{\partial u}{\partial x} = A_{22}^* f_{,yy} - A_{21}^* f_{,xx} - B_{21}^* \phi_{x,x} - B_{22}^* \phi_{y,y} + c_1 D_{21}^* \left(\phi_{x,x} + w_{,xx}\right) + c_1 D_{22}^* \left(\phi_{y,y} + w_{,yy}\right) \\
&+ \frac{w}{R_x} - \frac{1}{2}\left(\frac{\partial w}{\partial x}\right)^2 - \frac{\partial w}{\partial x}\frac{\partial w^*}{\partial x} + \left[A_{22}^*\left(\Phi_a^1 + \Phi_a^2\right) - A_{21}^*\left(\Phi_a^3 + \Phi_a^4\right)\right]\Delta T, \\
&\frac{\partial v}{\partial y} = A_{11}^* f_{,xx} - A_{12}^* f_{,yy} - B_{11}^* \phi_{x,x} + B_{11}^* \phi_{y,y} - c_1 D_{11}^* \left(\phi_{x,x} + w_{,xx}\right) - c_1 D_{12}^* \left(\phi_{y,y} + w_{,yy}\right) \\
&+ \frac{w}{R_y} - \frac{1}{2}\left(\frac{\partial w}{\partial y}\right)^2 - \frac{\partial w}{\partial x}\frac{\partial w^*}{\partial x} - \left[A_{12}^*\left(\Phi_a^1 + \Phi_a^2\right) - A_{11}^*\left(\Phi_a^3 + \Phi_a^4\right)\right]\Delta T.
\end{aligned} \tag{37}$$

Putting the Eqs. (30) – (32) into the Eq. (37), then the results into Eq. (36) leads to

$$\begin{aligned}
N_{x0} &= \overline{m_1} W + \overline{m_2}\Phi_x + \overline{m_3}\Phi_y + \overline{m_4} W(W + 2W_0) + \overline{m_5}\Delta T, \\
N_{y0} &= \overline{m_1^*} W + \overline{m_2^*}\Phi_x + \overline{m_3^*}\Phi_y + \overline{m_4^*} W(W + 2W_0) + \overline{m_5^*}\Delta T,
\end{aligned} \tag{38}$$

where

$$\Delta_1 = q_2^* q_2 - q_1^* q_1,\ \overline{m_1} = \frac{q_2 m_1^* + q_1^* m_1}{\Delta_1},\ \overline{m_2} = \frac{q_2 m_2^* + q_1^* m_2}{\Delta_1},\ \overline{m_3} = \frac{q_2 m_3^* + q_1^* m_3}{\Delta_1},$$
$$\overline{m_4} = \frac{q_2 m_4^* + q_1^* m_4}{\Delta_1},\ \overline{m_5} = \frac{q_2 m_5^* + q_1^* m_5}{\Delta_1},\ \overline{m_1^*} = \frac{q_1 m_1^* + m_1 q_2^*}{\Delta_1},\ \overline{m_2^*} = \frac{q_1 m_2^* + m_2 q_2^*}{\Delta_1},\tag{39}$$
$$\overline{m_3^*} = \frac{q_1 m_3^* + m_3 q_2^*}{\Delta_1},\ \overline{m_4^*} = \frac{q_1 m_4^* + m_4 q_2^*}{\Delta_1},\ \overline{m_5^*} = \frac{q_1 m_5^* + m_5 q_2^*}{\Delta_1}.$$

and $m_i,\ m_i^*\ (i = \overline{1,5}),\ q_j, q_j^*\ (j = 1,2)$ are given in Appendix C.

Introduction of Eqs. (38) into Eq. (35), yields

$$\begin{aligned} &L_{11}W + L_{12}\Phi_x + L_{13}\Phi_y + L_{14}\Phi_x\left(W + W_0\right) + L_{15}\Phi_y\left(W + W_0\right) + \left(n_1 + r_1\right)\left(W + W_0\right) \\ &+ r_2 W\left(W + W_0\right) + r_3 W\left(W + 2W_0\right) + r_4 W\left(W + W_0\right)\left(W + 2W_0\right) \\ &+ r_5 + n_5 q = I_1 \frac{\partial^2 W}{\partial t^2} + 2\varepsilon I_1 \frac{\partial W}{\partial t} - \alpha \overline{\overline{I}}_5 \frac{\partial^2 \Phi_x}{\partial t^2} - \beta \overline{\overline{I}}_5^* \frac{\partial^2 \Phi_y}{\partial t^2}, \end{aligned}\tag{40a}$$

$$J_{21}W + J_{22}\Phi_x\left(t\right) + J_{23}\Phi_y\left(t\right) + n_6\left(W + W_0\right) + n_7 W\left(W + 2W_0\right) = \overline{\overline{I}}_3 \frac{\partial^2 \Phi_x}{\partial t^2} - \alpha \overline{\overline{I}}_5 \frac{\partial^2 W}{\partial t^2},\tag{40b}$$

$$J_{31}W + J_{32}\Phi_x\left(t\right) + J_{33}\Phi_y\left(t\right) + n_8\left(W + W_0\right) + n_9 W\left(W + 2W_0\right) = \overline{\overline{I}}_3^* \frac{\partial^2 \Phi_y}{\partial t^2} - \beta \overline{\overline{I}}_5^* \frac{\partial^2 W}{\partial t^2},\tag{40c}$$

where

$$\begin{aligned} &L_{11} = \left(J_{11} + n_5 \frac{1}{R_x}\overline{m_1} + n_5 \frac{1}{R_y}\overline{m_1^*}\right),\ L_{12} = \left(J_{12} + n_5 \frac{1}{R_x}\overline{m_2} + n_5 \frac{1}{R_y}\overline{m_2^*}\right), \\ &L_{13} = \left(J_{13} + n_5 \frac{1}{R_x}\overline{m_3} + n_5 \frac{1}{R_y}\overline{m_3^*}\right),\ L_{14} = \left(J_{14} - \frac{ab}{4}\alpha^2 \overline{m_2} - \frac{ab}{4}\beta^2 \overline{m_2^*}\right), \\ &L_{15} = \left(J_{15} - \frac{ab}{4}\alpha^2 \overline{m_3} - \frac{ab}{4}\beta^2 \overline{m_3^*}\right),\ r_1 = \left(-\frac{ab}{4}\alpha^2 \overline{m_5} - \frac{ab}{4}\beta^2 \overline{m_5^*}\right), \\ &r_2 = \left(n_2 - \frac{ab}{4}\alpha^2 \overline{m_1} - \frac{ab}{4}\beta^2 \overline{m_1^*}\right),\ r_3 = \left(n_3 + n_5 \frac{1}{R_x}\overline{m_4} + n_5 \frac{1}{R_y}\overline{m_4^*}\right), \\ &r_4 = \left(n_4 - \frac{ab}{4}\alpha^2 \overline{m_4} - \frac{ab}{4}\beta^2 \overline{m_4^*}\right),\ r_5 = \left(n_5 \frac{1}{R_x}\overline{m_5} + n_5 \frac{1}{R_y}\overline{m_5^*}\right). \end{aligned}\tag{41}$$

The above system equations are basic equations which are used to investigate the

nonlinear dynamic response and vibration of the imperfect nanocomposite double curved shallow shells on the elastic foundations with immovable edges subjected to uniformly distributed pressure, thermal and damping loads. These equations could be solved by using the fourth – order Runge – Kutta method with the initial conditions are chosen as

$$W(0)=0,\Phi_x(0)=0,\Phi_y(0)=0 \text{ and } \frac{dW}{dt}(0)=0,\frac{d\Phi_x}{dt}(0)=0,\frac{d\Phi_y}{dt}(0)=0.$$

4.3. Natural frequency

In the case of free and linear vibration, the natural frequencies of the perfect nanocomposite double curved shallow shell are the smallest values of the axial, circumferential and radial directions which can be determined by solving the following determinant

$$\begin{vmatrix} L_{11}+n_1+r_1+I_1\omega^2 & L_{12}-\alpha\overline{\overline{I}}_5\omega^2 & L_{14}-\beta\overline{\overline{I}}_5^*\omega^2 \\ J_{21}+n_6-\alpha\overline{\overline{I}}_5\omega^2 & J_{22}+\overline{\overline{I}}_3\omega^2 & J_{23} \\ J_{31}+n_8-\beta\overline{\overline{I}}_5^*\omega^2 & J_{32} & J_{33}+\overline{\overline{I}}_3^*\omega^2 \end{vmatrix}=0. \quad (42)$$

5. Numerical results and discussion

5.1. Validation

To validate the accuracy of the present approach, the results of the fundamental frequency for the square plates and the nonlinear dynamic response of the double curved shallow shells are compared with other studies.

Firstly, Table 1 shows the comparison of the fundamental natural parameter $\Omega=\omega(b^2/h)\sqrt{\rho_m/E_m}$ for CNTRC double curved shell ($a/b=1,a/R_x=1,b/R_y=1/2,$ $b/h=10,h=1mm,\Delta T=0$) in this paper with the results in (Shen and He, 2017) based on the higher order deformation shell theory with different values of volume fraction CNT V_{CNT}^*, modes m,n and types of FG-CNTRC. It is easy to see a very good agreement in this comparison study.

Table 1. Comparison of the fundamental natural parameter $\Omega = \omega(b^2/h)\sqrt{\rho_c/E_c}$ for CNTRC double curved shells ($a/b=1, a/R_x=1, b/R_y=1/2, b/h=10, h=1mm$).

(m,n)	V_{CNT}^*	Ω	UD	$FG-V$	$FG-\Lambda$	$FG-X$
(1,1)	0.12	Shen and He (2017)	12.5022	11.6320	13.2122	16.5508
		Present	12.4872	11.0238	12.8605	16.2241
	0.17	Shen and He (2017)	15.6968	14.5319	16.3159	20.6753
		Present	15.8814	14.0843	15.8927	20.1793
	0.28	Shen and He (2017)	17.6011	16.5070	19.2067	23.5531
		Present	17.2216	16.1794	18.8433	23.1640
(1,3)	0.12	Shen and He (2017)	27.0617	26.4172	30.5916	35.9614
		Present	26.6825	25.8692	29.8258	35.6402
	0.17	Shen and He (2017)	34.8137	34.0998	38.8197	45.7687
		Present	34.7901	33.5290	38.2176	45.6503
	0.28	Shen and He (2017)	36.8280	36.6022	43.0309	53.0948
		Present	36.4659	36.2307	42.8946	52.5474

Next, Fig. 2 compares the nonlinear dynamic responses of the double curved shallow shell without elastic foundations subjected to uniformly distributed pressure and damping load in this paper with the results presented in (Bich et al., 2014) using the first order shear deformation shell theory. The input data are chosen as: $N=0,\ b/h=20,\ b/a=1,\ R_x=R_y=6\,m,\ k_1=k_2=0,\ W_0=0,\ \varepsilon=0.1,\ q=5000\sin(500t)$. As can be seen that there is a little difference between the results in this paper and those determined in existing publication.

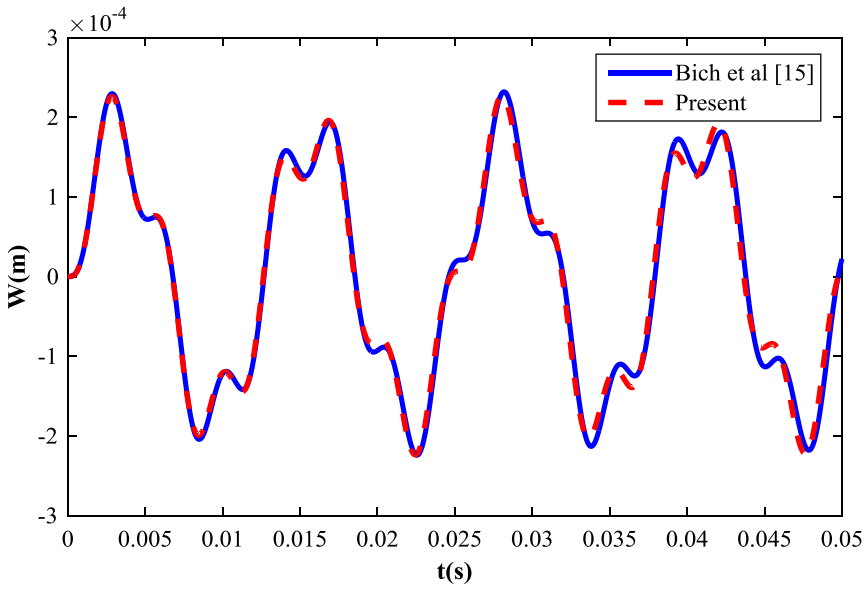

Fig. 1. Comparison of nonlinear dynamic responses of FGM double curved shallow shell subjected to mechanical and damping loads.

5.2. Natural frequency

Table 2 shows the effects of types of FG-CNTRC and ratio b/a on the natural frequency of the FG-CNTRC double curved shallow shells with $a/h = 30$, $R_x/h = R_y/h = 1500$, $k_1 = 10^9\, Pa/m$, $k_2 = 10^6\, Pa.m$, $\Delta T = 200K$. Five types of FG-CNTRC (FG-Λ, FG-O, UD, FG-X, FG-V) are considered. From the results in this table, it is observed that the value of the natural oscillation frequency of FG-CNTRC double curved shallow shells increases when the ratio b/a increases. Moreover, the natural oscillation frequency of FGV-CNTRC double curved shallow shell is highest and the natural oscillation frequency of FGΛ -CNTRC double curved shallow shell is lowest of all. Furthermore, natural oscillation frequency of FGX-CNTRC double curved shallow shell is higher than that of UD-CNTRC double curved shallow shell which is also higher than the frequency of FGO-CNTRC double curved shallow shell.

Table 2. Influences of type of FG-CNTRC and ratio b/a on the natural frequency of FG-CNTRC double curved shallow shells.

b/a	FG-A	FG-O	UD	FG-X	FG-V
1	2732	2927.6	2929.9	2931.9	3109.8
2	2659.3	2859.5	2863.9	2867.6	3049
3	2616	2819.1	2824	2828.0	3011.6
4	2576.3	2782.1	2787.3	2791.4	2977.2
5	2537.1	2745.8	2751.2	2755.4	2943.3
6	2497.8	2709.4	2714.9	2719.2	2909.4

The influences of volume fraction CNT, ratio R_x/h, temperature increment and elastic foundations on the natural frequency of the FGX-CNTRC double curved shallow shells are indicated in Table 3 with $a/h=30$ and $b/a=1$. Obviously, an increase of ratio R_x/h leads to an increase of the natural oscillation frequency of the FGX-CNTRC double curved shallow shells. Next, the natural oscillation frequency of FGX-CNTRC double curved shallow shells increases when the volume fraction CNT increases. In other words, carbon nanotubes have positive effect on the natural oscillation frequency of the FGX-CNTRC double curved shallow shell. In contrast, temperature increment has negative effect on the natural oscillation frequency of the FGX-CNTRC double curved shallow shells; when the temperature increment increases, the natural oscillation frequency of FGX-CNTRC double curved shallow shells decrease. The effect of elastic foundations with coefficients k_1, k_2 of the Winkler and Pasternak foundations on the natural oscillation frequency of FGX-CNTRC double curved shallow shells is also considered in Table 3. It can be seen that the natural frequencies of FGX-CNTRC double curved shallow shells on elastic foundations are greater than one of FGX-CNTRC double curved shallow shells without elastic foundations. The effect of elastic foundations on the natural frequencies of FGX-CNTRC double curved shallow shells are also shown specifically in Table 4 with various values of modulus k_1 and k_2. Clearly, the natural

frequency of FGX-CNTRC double curved shallow shells increases when the modulus k_1 and k_2 increase. Furthermore, the Pasternak foundation with modulus k_2 has stronger effect on the natural frequency of the shell than the Winkler foundation with modulus k_1.

Table 3. Effect of volume fraction CNT, elastic foundations, ratio R_x / h and temperature increment ΔT on the natural frequency of FGX-CNTRC double curved shallow shells.

$\Delta T(K)$	R_x / h	$k_1 = 0, k_2 = 0$			$k_1 = 10^9\ Pa.m, k_2 = 10^6\ Pa/m$		
		$V^*_{CNT} = 0.12$	$V^*_{CNT} = 0.17$	$V^*_{CNT} = 0.28$	$V^*_{CNT} = 0.12$	$V^*_{CNT} = 0.17$	$V^*_{CNT} = 0.28$
0	100	1588.2	1933.7	2374.8	3319.6	3485.2	3723
	400	1261.2	1547.5	1875.7	3176.2	3286.7	3426.3
	800	1246.3	1530.1	1853	3170.4	3278.5	3413.9
100	100	1512.8	1887.1	2246	3295.3	3459.8	3708.6
	400	1129.6	1474.5	1763.2	3085.1	3247.2	3369.9
	800	1217.8	1476.4	1702.3	3159.5	3201.8	3350.2
200	100	1420.4	1797.3	2196.4	3276.2	3378.5	3682.3
	400	1076.3	1378.9	1686.4	3026.5	3186.3	3309.8
	800	1173.6	1354.8	1627	3139.2	3178.6	3267.1

Table 4. Effect of elastic foundations on the natural frequency of FGX-CNTRC double curved shallow shells.

$k_1(GPa/m)$ \ $k_2(GPa.m)$	0	0.01	0.02	0.03	0.04	0.05
0	2.8152	3.1950	3.5343	3.8438	4.1302	4.3979
0.1	2.8873	3.2587	3.5920	3.8969	4.1797	4.4445
0.2	2.9576	3.3212	3.6488	3.9493	4.2286	4.4905
0.3	3.0263	3.3826	3.7047	4.0011	4.2769	4.5361
0.4	3.0935	3.4428	3.7598	4.0522	4.3248	4.5812

0.5	3.1593	3.5021	3.8141	4.1026	4.3721	4.6259

5.3. Nonlinear dynamic responses

In this section, we will consider the effect of geometrical parameters, temperature increment, elastic foundations, initial imperfection, mechanical loads, nanotube volume fraction and types of FG-CNTRC on the nonlinear dynamic response of imperfect nanocomposite double curved shallow shells. The thickness of FGX-CNTRC double curved shallow shells is $h = 0.01m$.

Effect of geometrical parameters

Figs. 3 and 4 indicate the effects of geometrical parameters a/h and b/a on the nonlinear dynamic response of imperfect FGX-CNTRC double curved shallow shells on elastic foundations subjected to uniformly distributed pressure in thermal environment, respectively. Obviously, the fluctuation amplitude of the imperfect FGX-CNTRC double curved shallow shells increases when increasing the ratio a/h and the ratio b/a.

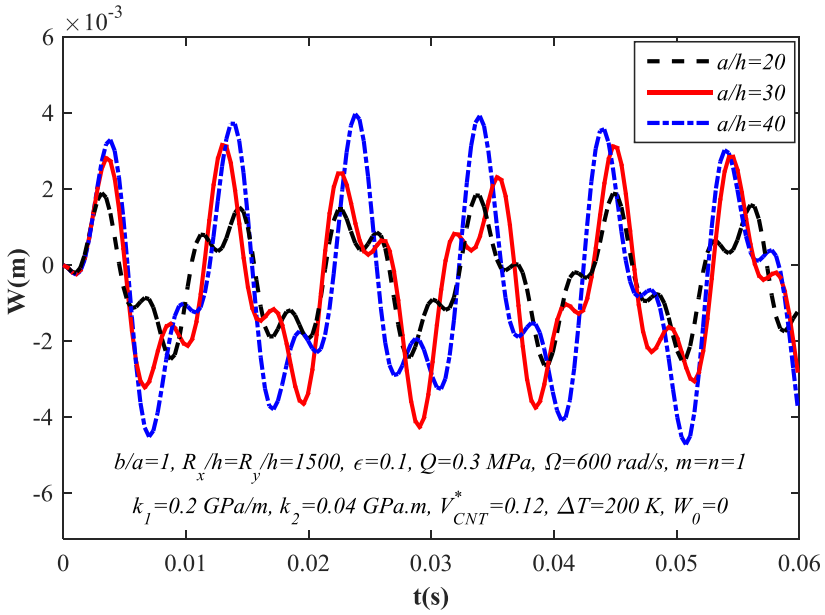

Fig. 3. Effect of ratio a/h on the nonlinear dynamic response of the imperfect FGX-CNTRC double curved shallow shell in thermal environments.

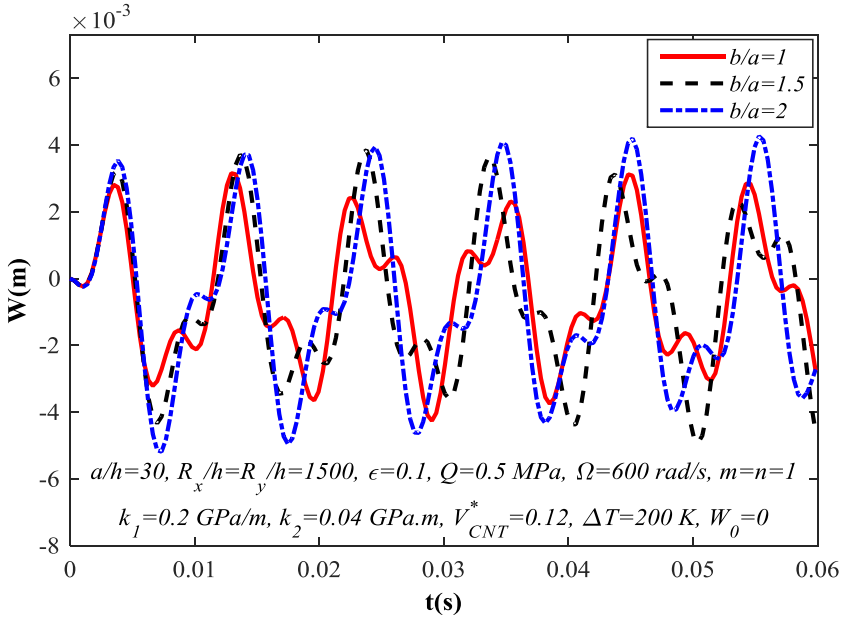

Fig. 4. Effect of ratio b/a on the nonlinear dynamic response of the imperfect FGX-CNTRC double curved shallow shell in thermal environments.

Effect of temperature increment

Fig. 5 shows the effect of temperature increment ΔT on the nonlinear dynamic response of the imperfect FGX-CNTRC double curved shallow shell in thermal environments with $a/h = b/h = 30,\ R_x/h = R_y/h = 1500, V_{CNT}^* = 0.12, \varepsilon = 0.1$. It can be seen that the temperature increment ΔT has negative effect on the nonlinear dynamic response of FGX-CNTRC double curved shallow shells. Specifically, FGX-CNTRC double curved shallow shell fluctuation amplitude increases when the temperature increment ΔT increases.

Effect of exciting force amplitude

The nonlinear dynamic response of FGX-CNTRC double curved shallow shells on elastic foundations subjected to mechanical load and temperature with different values of exciting force amplitude Q is illustrated in Fig. 6. As can be observed, an increase of the amplitude of uniformly distributed pressure Q leads to an increase of nonlinear dynamic response amplitude of the FGX-CNTRC double curved shallow shell.

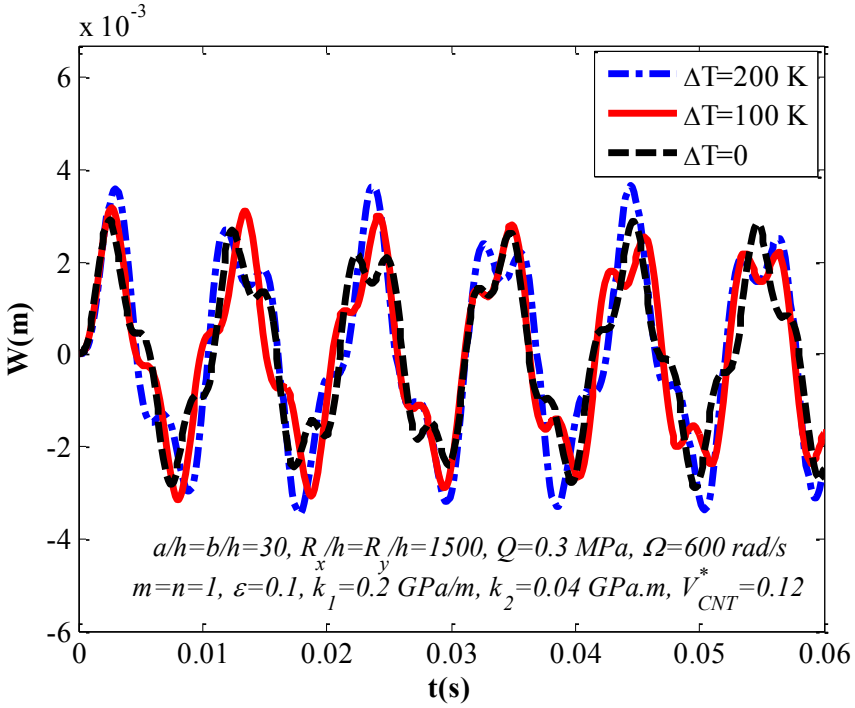

Fig. 5. Effect of temperature increment ΔT on the nonlinear dynamic response of the imperfect FGX-CNTRC double curved shallow shell in thermal environments.

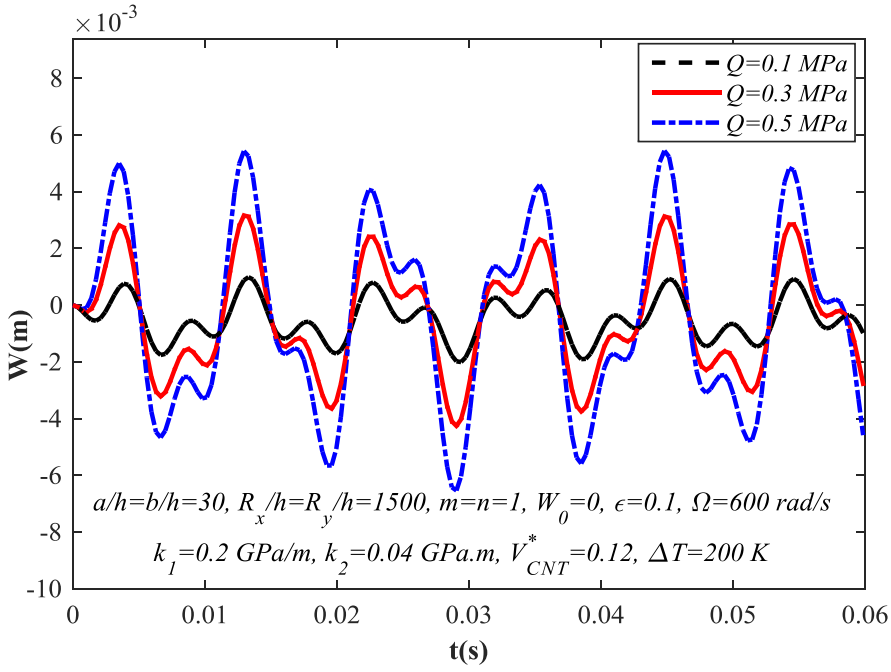

Fig. 6. Effect of exciting force amplitude Q on the nonlinear dynamic response of the imperfect FGX-CNTRC double curved shallow shell in thermal environments.

Effect of initial imperfection

The influences of initial imperfection with amplitude W_0 on the nonlinear dynamic response of FGX-CNTRC double curved shallow shells subjected to uniformly distributed pressure, thermal and damping loads are shown in Fig. 7. Three values of amplitude of initial imperfection $W_0 : 0, 0.001m$ and $0.002\,m$ are used. It can be seen that the nonlinear dynamic response amplitude of the FGX-CNTRC double curved shallow shell increased when the amplitude W_0 increased.

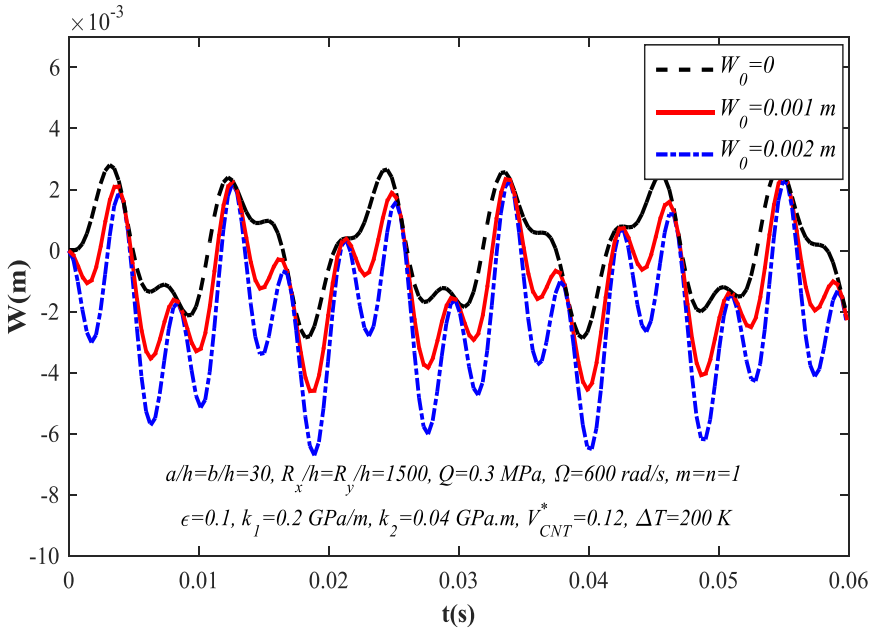

Fig. 7. Effects of initial imperfection on the nonlinear dynamic response of the imperfect FGX-CNTRC double curved shallow shell in thermal environments.

Effects of elastic foundations

Figs. 8 and 9 indicate the effects of elastic foundations on the nonlinear dynamic response of the FGX-CNTRC double curved shallow shells under uniform external pressure in thermal environments. As expected, the nonlinear dynamic amplitude of the panel becomes considerably lower due to the support of elastic foundations. Furthermore,

the beneficial effect of the Pasternak foundation on the nonlinear dynamic response of the FGX-CNTRC double curved shallow shells is better than the Winkler one.

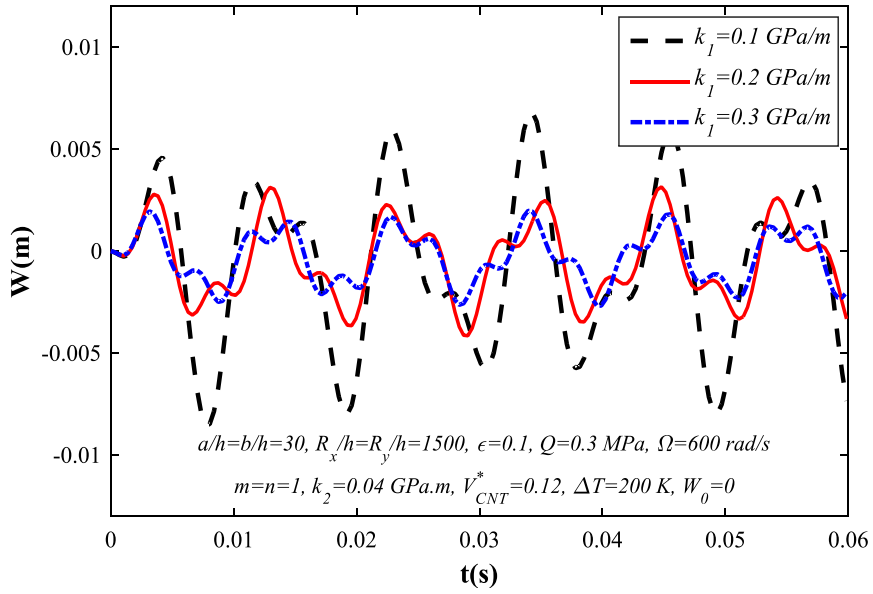

Fig. 8. Effect of Winkler foundation on the nonlinear dynamic response of the imperfect FGX-CNTRC double curved shallow shell in thermal environments.

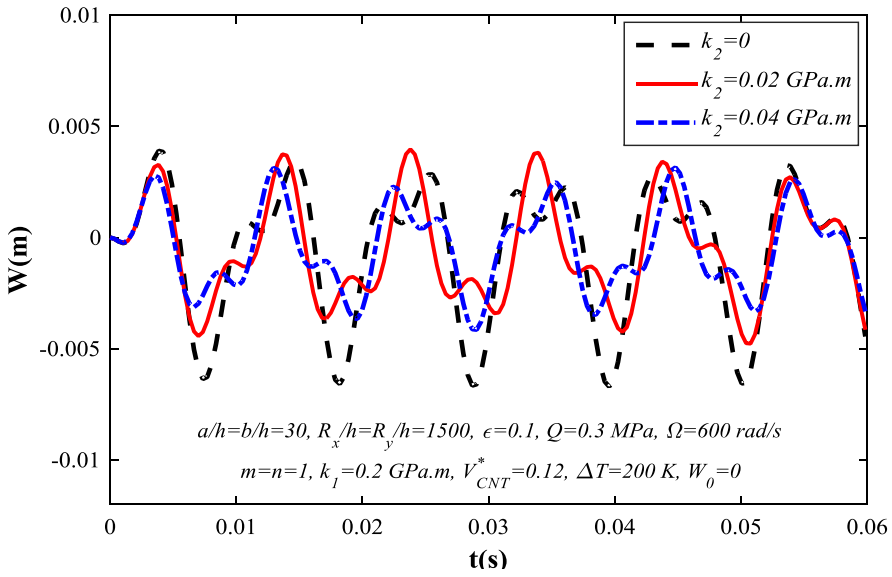

Fig. 9. Effect of Pasternak foundation on the nonlinear dynamic response of the imperfect FGX-CNTRC double curved shallow shell in thermal environments.

Effect of carbon nanotube volume fraction

Fig. 10 considers the nonlinear dynamic response of the imperfect FGX-CNTRC double curved shallow shells in thermal environments with different values of carbon nanotube volume fraction (V_{CNT}^{*}). The input data are: $a/b=1$, $b/h=30$, $R_x/h=R_y/h=1500$, $\varepsilon=0.1, W_0=0$. As shown, the higher the carbon nanotube volume fraction is, the lower the amplitude of the FGX-CNTRC double curved shallow shells is. In other words, carbon nanotubes play an important role in increasing the stiffness of FGX-CNTRC double curved shallow shells.

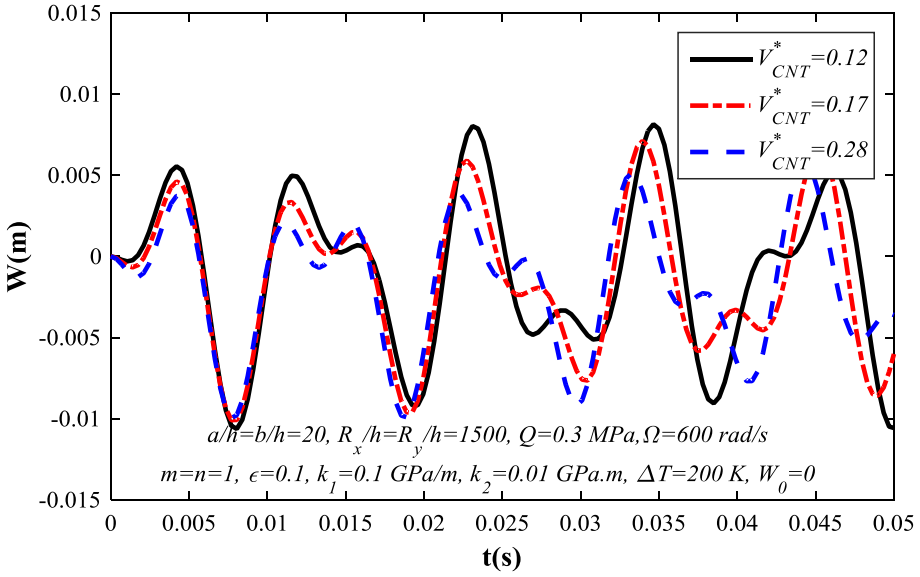

Fig. 10. Effects of CNT volume fraction on the nonlinear dynamic response of the imperfect FGX-CNTRC double curved shallow shells in thermal environments.

Effect of types of FG-CNTRC

Fig. 11 gives comparison of the nonlinear amplitude fluctuation for FG-CNTRC double curved shallow shells of type X, O and UD subjected to uniformly distributed pressure, thermal and damping loads with the same geometrical parameters. Clearly, the amplitude fluctuation of FGX-CNTRC double curved shallow shell is highest of all and the amplitude fluctuation of FGX-CNTRC double curved shallow shell is lowest of all.

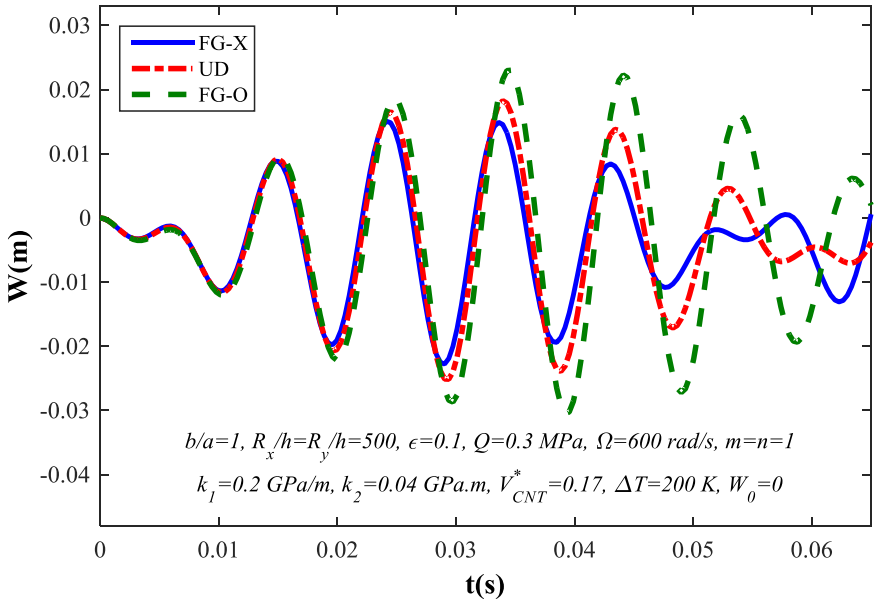

Fig. 11. Effects of type of CNT reinforcements on the nonlinear dynamic response of the imperfect FG-CNTRC double curved shallow shells in thermal environments.

6. Conclusions

This paper used the stress method to investigate the nonlinear dynamic response and vibration of nanocomposite (FG-CNTRC) double curved shallow shells on elastic foundations subjected to combination of mechanical, thermal and damping loads. Governing equations are derived using Reddy's higher order shear deformation shell theory taking into account geometrical nonlinearity and temperature dependent properties. One-term approximate solutions are assumed to satisfy simply supported boundary conditions. The full order equations are obtained by using Galerkin method then Runge – Kutta method is used to give the nonlinear dynamic responses of the nanocomposite shells. Numerical results show the positive effects of elastic foundations and carbon nanotubes as well as the negative influence of temperature increment and initial imperfection on the nonlinear vibration of the nanocomposite double curved shallow shells. While elastic foundations and carbon nanotubes enhance the stiffness, increase the natural frequency and decrease the nonlinear dynamic response amplitude of the nanocomposite shells, the temperature increment and initial imperfection increase the

amplitude and reduce the natural frequency of the shell. The influences of geometrical parameters and the type of FG-CNTRC on nonlinear vibration of the nanocomposite double curved shallow shells are also studied and discussed in details. The present approach and theory are validated by comparing with results of other authors.

Funding: This research is funded by the National Science and Technology Program of Vietnam for the period of 2016-2020 "Research and development of science education to meet the requirements of fundamental and comprehensive reform education of Vietnam" under Grant number KHGD/16-20.ĐT.032. The authors are grateful for this support.

Conflict of interest statement: The authors declare no conflict of interest.

Appendix A

$$X_{11} = S_{44} - 3c_1 Z_{44},\ X_{12} = S_{55} - 3c_1 Z_{55},\ X_{13} = V_{31},\ X_{14} = V_{32} + 4V_{66}^* + V_{41},\ X_{15} = V_{42},$$
$$X_{16} = c_1\left(Z_{31} + V_{31}\right),\ X_{17} = c_1\left(2Z_{66}^* + 2V_{66}^* + Z_{41} + V_{41}\right), X_{18} = c_1\left(Z_{42} + V_{42}\right),$$
$$X_{19} = c_1\left(Z_{32} + V_{32} + 2Z_{66}^* + 2V_{66}^*\right),\ X_{110} = c_1 S_{31},\ X_{111} = c_1 S_{32} - 2c_1 S_{66}^* + S_{41}c_1,\ X_{112} = S_{42}c_1,$$
$$X_{21} = 3c_1 Z_{44} - S_{44},\ X_{22} = V_{11} - c_1 V_{31},\ X_{23} = V_{12} + 2V_{66} - 2c_1 V_{66}^* - c_1 V_{32},$$
$$X_{24} = Z_{11} + V_{11} - c_1 V_{31} - c_1 Z_{31}, X_{25} = V_{66} + Z_{66} - c_1 Z_{66}^* - c_1 V_{66}^* - c_1 Z_{32},$$
$$X_{26} = Z_{12} + V_{12} + Z_{66} + V_{66} - c_1 V_{32} - c_1 Z_{66}^* - c_1 V_{66}^*,$$
$$X_{27} = S_{11} + c_1 S_{66}^*,\ X_{28} = S_{12} - S_{66} - c_1 S_{32} + c_1 S_{66}^*,$$
$$X_{31} = \left(3c_1 Z_{55} - S_{55}\right),\ X_{32} = \left(2V_{66} + V_{21}c_1 - 2c_1 V_{66}^* - c_1 V_{41}\right),\ X_{33} = \left(V_{22}c_1 - c_1 V_{42}\right),$$
$$X_{34} = \left(Z_{66} + V_{66} - c_1 Z_{66}^* - c_1 V_{66}^* + Z_{21} + V_{21}c_1 - c_1 Z_{41} - c_1 V_{41}\right),\ X_{35} = \left(Z_{66} + V_{66} - c_1 Z_{66}^* - c_1 V_{66}^*\right),$$
$$X_{36} = \left(Z_{22} + V_{22}c_1 - c_1 Z_{42} - c_1 V_{42}\right),\ X_{37} = \left(S_{21} - S_{66} + c_1 S_{66}^* - c_1 S_{41}\right),\ X_{38} = \left(S_{22} - c_1 S_{42}\right),$$

with

$$S_{11} = \left(B_{12}A_{11}^* - B_{11}A_{21}^*\right); S_{12} = \left(B_{11}A_{22}^* - B_{12}A_{12}^*\right); Z_{11} = \left(B_{12}B_{11}^* - B_{11}B_{21}^* + C_{11}\right);$$
$$Z_{12} = \left(B_{12}B_{12}^* - B_{11}B_{22}^* + C_{12}\right); V_{11} = c_1\left(B_{11}D_{21}^* - B_{12}D_{11}^* - E_{11}\right); V_{12} = c_1\left(B_{11}D_{22}^* - B_{12}D_{12}^* - E_{12}\right)$$
$$S_{21} = \left(B_{22}A_{11}^* - B_{12}A_{21}^*\right),\ S_{22} = \left(B_{12}A_{22}^* - B_{22}A_{12}^*\right),\ Z_{21} = \left(B_{22}B_{11}^* - B_{12}B_{21}^* + C_{12}\right),$$
$$Z_{22} = \left(B_{22}B_{12}^* - B_{12}B_{22}^* + C_{22}\right), V_{21} = c_1\left(B_{12}D_{21}^* - B_{22}D_{11}^* - E_{12}\right), V_{22} = c_1\left(B_{12}D_{22}^* - B_{22}D_{12}^* - E_{22}\right),$$
$$S_{31} = \left(D_{12}A_{11}^* - D_{11}A_{21}^*\right),\ S_{32} = \left(D_{11}A_{22}^* - D_{12}A_{12}^*\right),\ Z_{31} = \left(D_{12}B_{11}^* - D_{11}B_{21}^* + E_{11}\right),$$
$$Z_{32} = \left(D_{12}B_{12}^* - D_{11}B_{22}^* + E_{12}\right), V_{31} = c_1\left(D_{11}D_{21}^* - D_{12}D_{11}^* - G_{11}\right), V_{32} = c_1\left(D_{11}D_{22}^* - D_{12}D_{12}^* - G_{12}\right),$$

$S_{41} = \left(D_{22}A_{11}^{*} - D_{12}A_{21}^{*}\right),\ S_{42} = \left(D_{12}A_{22}^{*} - D_{22}A_{12}^{*}\right),\ Z_{41} = \left(D_{22}B_{11}^{*} - D_{12}B_{21}^{*} + E_{12}\right),$

$Z_{42} = \left(D_{22}B_{12}^{*} - D_{12}B_{22}^{*} + E_{22}\right),\ V_{41} = c_1\left(D_{12}D_{21}^{*} - D_{22}D_{11}^{*} - G_{12}\right),\ V_{42} = c_1\left(D_{12}D_{22}^{*} - D_{22}D_{12}^{*} - G_{22}\right),$

$S_{66} = B_{66}A_{66}^{*},\ Z_{66} = \left(C_{66} - B_{66}B_{66}^{*}\right);V_{66} = c_1\left(B_{66}D_{66}^{*} - E_{66}\right),\ S_{66}^{*} = D_{66}A_{66}^{*},\ Z_{66}^{*} = \left(E_{66} - D_{66}B_{66}^{*}\right),$

$V_{66}^{*} = c_1\left(D_{66}D_{66}^{*} - G_{66}\right),\ Z_{44} = \left(C_{44} - 3c_1E_{44}\right),\ Z_{55} = \left(C_{55} - 3c_1E_{55}\right).$

Appendix B

$J_{11} = U_{143}\frac{H_4}{H_1},\ J_{12} = \left(U_{12} + U_{143}\frac{H_2}{H_1}\right),\ J_{13} = \left(U_{13} + U_{143}\frac{H_3}{H_1}\right),$

$J_{14} = \left(\alpha^2\beta^2\frac{32ab}{9\pi^2} - 2\alpha^2\beta^2\frac{4ab}{9\pi^2}\right)\frac{H_2}{H_1}\frac{4}{ab},\ J_{15} = \left(\alpha^2\beta^2\frac{32ab}{9\pi^2} - 2\alpha^2\beta^2\frac{4ab}{9\pi^2}\right)\frac{H_3}{H_1}\frac{4}{ab},$

$n_1 = U_{11},\ n_2 = \left(\alpha^2\beta^2\frac{32ab}{9\pi^2} - 2\alpha^2\beta^2\frac{4ab}{9\pi^2}\right)\frac{H_4}{H_1}\frac{4}{ab},\ n_3 = \frac{-4ab}{3\pi^2}\left(U_{141}\frac{\beta^2}{32\alpha^2A_{11}^{*}} + U_{142}\frac{\alpha^2}{32\beta^2A_{22}^{*}}\right)\frac{4}{ab},$

$n_4 = \frac{-ab}{2}\alpha^2\beta^2\left(\frac{\beta^2}{32\alpha^2A_{11}^{*}} + \frac{\alpha^2}{32\beta^2A_{22}^{*}}\right)\frac{4}{ab},\ n_5 = \frac{4ab}{\pi^2}\frac{4}{ab},\ J_{21} = U_{242}\frac{H_4}{H_1},\ J_{22} = \left[U_{22} + U_{242}\frac{H_2}{H_1}\right],$

$J_{23} = \left[U_{23} + U_{242}\frac{H_3}{H_1}\right],\ n_6 = U_{21},\ n_7 = U_{241}\frac{\beta^2}{32\alpha^2A_{11}^{*}}\frac{8ab}{3\pi^2},\ J_{31} = U_{341}\frac{H_4}{H_1},\ J_{32} = \left(U_{32} + U_{341}\frac{H_2}{H_1}\right),$

$J_{33} = \left(U_{33} + U_{341}\frac{H_3}{H_1}\right),\ n_8 = U_{31},\ n_9 = U_{342}\frac{\alpha^2}{32\beta^2A_{22}^{*}}\frac{8ab}{3\pi^2}\frac{4}{ab},$

with

$U_{11} = \left(-X_{11}\alpha^2 - X_{12}\beta^2 + X_{13}\alpha^4 + X_{14}\alpha^2\beta^2 + X_{15}\beta^4 - k_1 - k_2\alpha^2 - k_2\beta^2\right),$

$U_{12} = \left(-X_{11}\alpha + X_{16}\alpha^3 + X_{17}\alpha\beta^2\right),\ U_{13} = \left(-X_{12}\beta + X_{18}\beta^3 + X_{19}\alpha^2\beta\right),$

$U_{141} = \left(X_{110}(2\alpha)^4 - \frac{1}{R_y}(2\alpha)^2\right),\ U_{142} = \left(X_{112}(2\beta)^4 - \frac{1}{R_x}(2\beta)^2\right),$

$U_{143} = \left(X_{110}\alpha^4 + X_{111}\alpha^2\beta^2 + X_{112}\beta^3 - \frac{1}{R_x}\beta^2 - \frac{1}{R_y}\alpha^2\right),$

$U_{21} = \left(X_{21}\alpha - X_{22}\alpha^3 - X_{23}\alpha\beta^2\right),\ U_{22} = \left(X_{21} - X_{24}\alpha^2 - X_{25}\beta^2\right),\ U_{23} = -X_{26}\alpha\beta,$

$U_{241} = X_{27}(2\alpha)^3,\ U_{242} = -\left(X_{27}\alpha^3 + X_{28}\alpha\beta^2\right),$

$U_{31} = \left(X_{31}\beta - X_{32}\alpha^2\beta - X_{33}\beta^3\right),\ U_{32} = -X_{34}\alpha\beta,\ U_{33} = \left(X_{31} - X_{35}\alpha^2 - X_{36}\beta^2\right),$

$U_{341} = -\left(X_{37}\alpha^2\beta + X_{38}\beta^3\right),\ U_{342} = X_{38}(2\beta)^3.$

Appendix C

$$q_1 = abA_{22}^*,\ q_2 = abA_{21}^*,\ q_1^* = abA_{11}^*,\ q_2^* = abA_{12}^*,$$

$$m_1 = \frac{4ab}{\pi^2}\left(A_{21}^*\alpha^2\frac{H_4}{H_1} - A_{22}^*\beta^2\frac{H_4}{H_1} + \frac{1}{R_x} - c_1D_{21}^*\alpha^2 - c_1D_{22}^*\beta^2 \right),$$

$$m_2 = \frac{4ab}{\pi^2}\left(A_{21}^*\alpha^2\frac{H_2}{H_1} - A_{22}^*\beta^2\frac{H_2}{H_1} + B_{21}^*\alpha - c_1D_{21}^*\alpha \right),$$

$$m_3 = \frac{4ab}{\pi^2}\left(A_{21}^*\alpha^2\frac{H_3}{H_1} - A_{22}^*\beta^2\frac{H_3}{H_1} + B_{22}^*\beta - c_1D_{22}^*\beta \right),$$

$$m_4 = -\frac{1}{2}\alpha^2\frac{ab}{4},\ m_5 = ab\left[A_{22}^*\left(\Phi_a^1 + \Phi_a^2\right) - A_{21}^*\left(\Phi_a^3 + \Phi_a^4\right)\right]\Delta T,$$

$$m_1^* = \frac{4ab}{\pi^2}\left(A_{12}^*\beta^2\frac{H_4}{H_1} - A_{11}^*\alpha^2\frac{H_4}{H_1} + \frac{1}{R_y} + c_1D_{11}^*\alpha^2 + c_1D_{12}^*\beta^2 \right),$$

$$m_2^* = \frac{4ab}{\pi^2}\left(A_{12}^*\beta^2\frac{H_2}{H_1} - A_{11}^*\alpha^2\frac{H_2}{H_1} + c_1D_{11}^*\alpha - B_{11}^*\alpha \right),$$

$$m_3^* = \frac{4ab}{\pi^2}\left(A_{12}^*\beta^2\frac{H_3}{H_1} - A_{11}^*\alpha^2\frac{H_3}{H_1} + c_1D_{12}^*\beta - B_{12}^*\beta \right),$$

$$m_4^* = -\frac{1}{2}\beta^2\frac{ab}{4};\ m_5^* = ab\left[A_{11}^*\left(\Phi_a^3 + \Phi_a^4\right) - A_{12}^*\left(\Phi_a^1 + \Phi_a^2\right)\right]\Delta T.$$

References

Anh, V.T.T., Bich, D.H., Duc, N.D., 2015. Nonlinear stability analysis of thin FGM annular spherical shells on elastic foundations under external pressure and thermal loads. European Journal of Mechanics, A/Solids 50, 28–38.

Asnafi, N., 2001. On springback of double-curved autobody panels. International Journal of Mechanical Sciences 43, 5-37.

Bich, D.H., Duc, N.D., Quan, T.Q., 2014. Nonlinear vibration of imperfect eccentrically stiffened functionally graded double curved shallow shells resting on elastic foundation using the first order shear deformation theory. International Journal of Mechanical Sciences 80, 16–28.

Bouras, Y., Vrcelj, Z., 2017. Non-linear in-plane buckling of shallow concrete arches subjected to combined mechanical and thermal loading. Engineering Structures 152, 413–423.

Brush, D.D., Almroth, B.O., 1975. Buckling of bars, plates and shells, Mc. Graw-Hill.

Cortsen, J., Rytz, J.A., Ellekilde, L.P., Sølvason, D., Petersen, H.G., 2014. Automated Fabrication of double curved reinforcement structures for unique concrete buildings. Robotics and Autonomous Systems 62, 1387–1397.

Dobrzańska-Danikiewicz, A.D., Wolany, W., Gołombek, K., 2017. Microscopic and spectroscopic investigation of carbon nanotubes-rhenium nanocomposites fabricated in different conditions. Archives of Civil and Mechanical Engineering 17, 978–985.

Dong, Y.H., Li, Y.H., 2017. A unified nonlinear analytical solution of bending, buckling and vibration for the temperature-dependent FG rectangular plates subjected to thermal load. Composite Structures 159, 689–701.

Duc, N.D., 2013. Nonlinear dynamic response of imperfect eccentrically stiffened FGM double curved shallow shells on elastic foundation. Composite Structures 102, 306-314.

Duc, N.D., Cong, P.H., Tuan, N.D., Tran, P., Thanh, N. Van, 2017. Thermal and mechanical stability of functionally graded carbon nanotubes (FG CNT)-reinforced composite truncated conical shells surrounded by the elastic foundations. Thin-Walled Structures 115, 300–310.

Duc, N.D., Quan, T.Q., 2015. Nonlinear dynamic analysis of imperfect FGM double curved thin shallow shells with temperature-dependent properties on elastic foundation. Vibration and Control 21 (7), 1340-1362.

Fontananova, E., Grosso, V., Aljlil, S.A., Bahattab, M.A., Vuono, D., Nicoletta, F.P., Curcio, E., Drioli, E., Di Profio, G., 2017. Effect of functional groups on the properties of multiwalled carbon nanotubes/polyvinylidenefluoride composite membranes. Journal of Membrane Science 541, 198–204.

Ghosh, S., Bhattacharya, P., 2015. Energy transmission through a double-wall curved

stiffened panel using Greens theorem. Journal of Sound and Vibration 342, 218–240.

Han, B., Qin, K.K., Zhang, Q.C., Zhang, Q., Lu, T.J., Lu, B.H., 2017. Free vibration and buckling of foam-filled composite corrugated sandwich plates under thermal loading. Composite Structures 172, 173–189.

Hosseini-Hashemi, Sh., Rokni Damavandi Taher, H., Akhavan, H., Omidi, M., 2010. Free vibration of functionally graded rectangular plates using first-order shear deformation plate theory. Applied Mathematical Modelling 34 (5), 127691.

Jakomin, M., Kosel, F., Kosel, T., 2010. Thin double curved shallow bimetallic shell of translation in a homogenous temperature field by non-linear theory. Thin-Walled Structures 48, 243–259.

Kateryna, D., Nataliia, K., 2015. Stress-deformable state of isotropic double curved shell with internal cracks and a circular hole. Mechanics of Materials 90, 111–117.

Li, J., Zhang, F., Wang, C., Shao, C., Li, B., Li, Y., Wu, Q.-H., Yang, Y., 2017. Self nitrogen-doped carbon nanotubes as anode materials for high capacity and cycling stability lithium-ion batteries. Materials & Design 133, 169–175.

Li, Y., Wang, Z.J., 2009. Finite element analysis of stiffness and static dent resistance of aluminum alloy double-curved panel in viscous pressure forming. Transactions of Nonferrous Metals Society of China (English Edition) 19, s312–s317.

Liu, Z., Li, L., Zhao, Z., Liu, Y., Lu, M., 2017. Antistatic silk fabric through sericin swelling-fixing treatment with aminated carbon nanotubes. Materials Science and Engineering: B 226, 72–77.

Liu, B.,, Dui, G.,, Yang, S.,2013. On the transformation behavior of functionally graded SMA composites subjected to thermal loading. European Journal of Mechanics - A/Solids 40, 139-147.

Lv, Q., Wang, Z., Chen, S., Li, C., Sun, S., Hu, S., 2017. Effects of single adatom and Stone-Wales defects on the elastic properties of carbon nanotube/polypropylene composites: A molecular simulation study. International Journal of Mechanical Sciences 131-132, 527–534.

Matsunaga, H., 2008. Free vibration and stability of functionally graded plates according to a 2-D higher-order deformation theory. Composite Structures 82, 499–512.

Pantano, A., 2017. Effects of mechanical deformation on electronic transport through multiwall carbon nanotubes. International Journal of Solids and Structures 122-123.

Quan, T.Q., Duc, N.D., 2017. Nonlinear thermal stability of eccentrically stiffened FGM double curved shallow shells. Thermal Stresses 40 (2), 211-236.

Reddy, J.N., 2004 Mechanics of laminated composite plates and shells: Theory and analysis, Boca Raton: CRC Press.

Sha, Y., Wang, J., 2017. Nonlinear response analysis and experimental verification for thin-walled plates to thermal-acoustic loads. Chinese Journal of Aeronautics.

Shen, H.S., 2009. Nonlinear bending of functionally graded carbon nanotube-reinforced composite plates in thermal environments. Composite Structures 91, 9–619.

Shen, H.S., He, X.Q., 2017. Large amplitude free vibration of nanotube-reinforced composite doubly curved panels resting on elastic foundations in thermal environments. Journal of Vibration and Control 23, 2672-2689.

Sheng, G.G., Wang, X., 2017. Nonlinear response of fluid-conveying functionally graded cylindrical shells subjected to mechanical and thermal loading conditions. Composite Structures 168, 675–684.

Thai, S., Thai, H.T., Vo, T.P., Reddy, J.N., 2017. Post-buckling of functionally graded microplates under mechanical and thermal loads using isogeomertic analysis. Engineering Structures 150, 905–917.

Weickgenannt, M., Neuhaeuser, S., Henke, B., Sobek, W., Sawodny, O., 2013. Optimal sensor placement for state estimation of a thin double-curved shell structure. Mechatronics 23, 346–354.

Xu, F., Abdelmoula, R., Potier-ferry, M., 2017. On the buckling and post-buckling of core-shell cylinders under thermal loading. International Journal of Solids and Structures 126-127, 17–36.

Zghal, S., Frikha, A., Dammak, F., 2017. Static analysis of functionally graded carbon

nanotube-reinforced plate and shell structures. Composite Structures 176, 1107–1123.